

**2021 Fall**

# **“Phase Transformation *in* Materials”**

**22<sup>nd</sup> lecture**

**Eun Soo Park**

**Office: 33-313**

**Telephone: 880-7221**

**Email: [espark@snu.ac.kr](mailto:espark@snu.ac.kr)**

**Office hours: by an appointment**

## Contents for previous class

### < Phase Transformation in Solids >

#### 1) Diffusional Transformation (a) Precipitation Nucleation & Growth

**Q1: Overall Transformation Kinetics–TTT diagram**

**“Johnson-Mehl-Avrami Equation”**

**Q2: Precipitation in Age-Hardening Alloys**

**Q3: Age Hardening**

- Precipitate growth**

- Growth behind Planar Incoherent Interfaces**

Diffusion-Controlled Thickening:  $x \propto \sqrt{(Dt)}$  Parabolic growth

$$v = \frac{D(\Delta C_0)^2}{2(C_\beta - C_e)(C_\beta - C_0)x}$$

$$v \propto \Delta X_0 \propto \sqrt{(D/t)}$$

Supersaturation

- Diffusion Controlled lengthening of Plates or Needles**

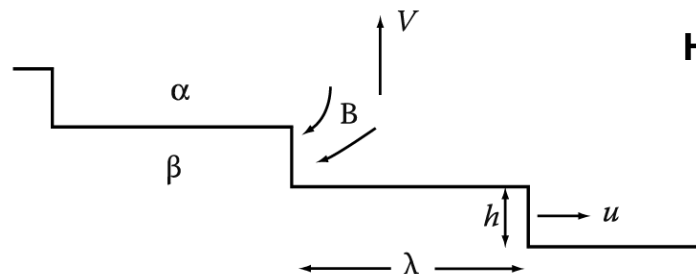
Diffusion Controlled lengthening:

$$v = \frac{D\Delta X_0}{k(X_\beta - X_r)} \cdot \frac{1}{r} \left( 1 - \frac{r^*}{r} \right)$$

$V \rightarrow \text{constant} \rightarrow X \propto t$   
Linear growth

- Thickening of Plate-like Precipitates**

Thickening of Plate-like Precipitates by Ledge Mechanism



Half Thickness Increase

$$v = \frac{uh}{\lambda}$$

$$v = \frac{D\Delta X_0}{k(X_\beta - X_e)\lambda}$$

$u$ : rate of lateral migration

# 5.4 Overall Transformation Kinetics – TTT Diagram

If isothermal transformation,

The fraction of Transformation as a function of Time and Temperature

$$\rightarrow f(t, T)$$

Plot  $f$  vs  $\log t$ .

- isothermal transformation
- $f \sim$  volume fraction of  $\beta$  at any time;  $0 \sim 1$

Plot the fraction of transformation (1%, 99%) in T-log t coordinate.

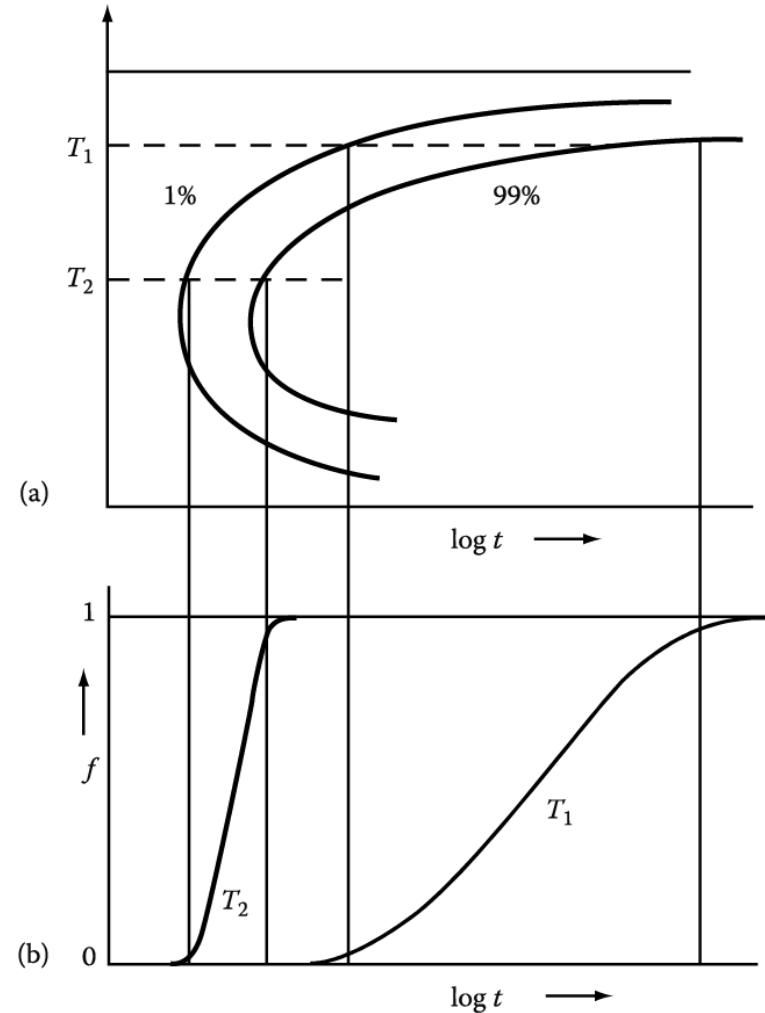


Fig. 5.23 The percentage transformation versus time for different transformation temperatures.

# Transformation Kinetics

- **Avrami proposed that for a three-dimensional nucleation and growth process kinetic law**

$$f = 1 - \exp(-kt^n) \quad \text{Johnson-Mehl-Avrami equation}$$

$f$  : volume fraction transformed =  $\frac{\text{Volume of new phase}}{\text{Volume of specimen}}$

- **Assumption :**
  - ✓ reaction produces by nucleation and growth
  - ✓ nucleation occurs randomly throughout specimen
  - ✓ reaction product grows rapidly until impingement

# Time-Temperature-Transformation Curves (TTT)

- How much time does it take at any one temperature for a given fraction of the liquid to transform (nucleate and grow) into a crystal?

- $f(t, T) \sim \pi I(T) \mu(T)^3 t^4 / 3$

where  $f$  is the fractional volume of crystals formed, typically taken to be  $10^{-6}$ , a barely observable crystal volume.

Nucleation rates

$$I = n \nu \exp \left\{ \left( \frac{16\pi\Delta H_{cryst}}{81RT} \right) \left( \frac{T_m}{\Delta T} \right)^2 \right\} \exp \left\{ \frac{-\Delta E_D}{RT} \right\}$$

Growth rates

$$\mu(T) = \left( \frac{fRT}{3N\pi a^2 \eta(T)} \right) \left( 1 - \exp \left[ \left( \frac{\Delta H_m}{RT} \right) \left( \frac{\Delta T}{T_m} \right) \right] \right)$$

# \* Time-Temperature-Transformation diagrams

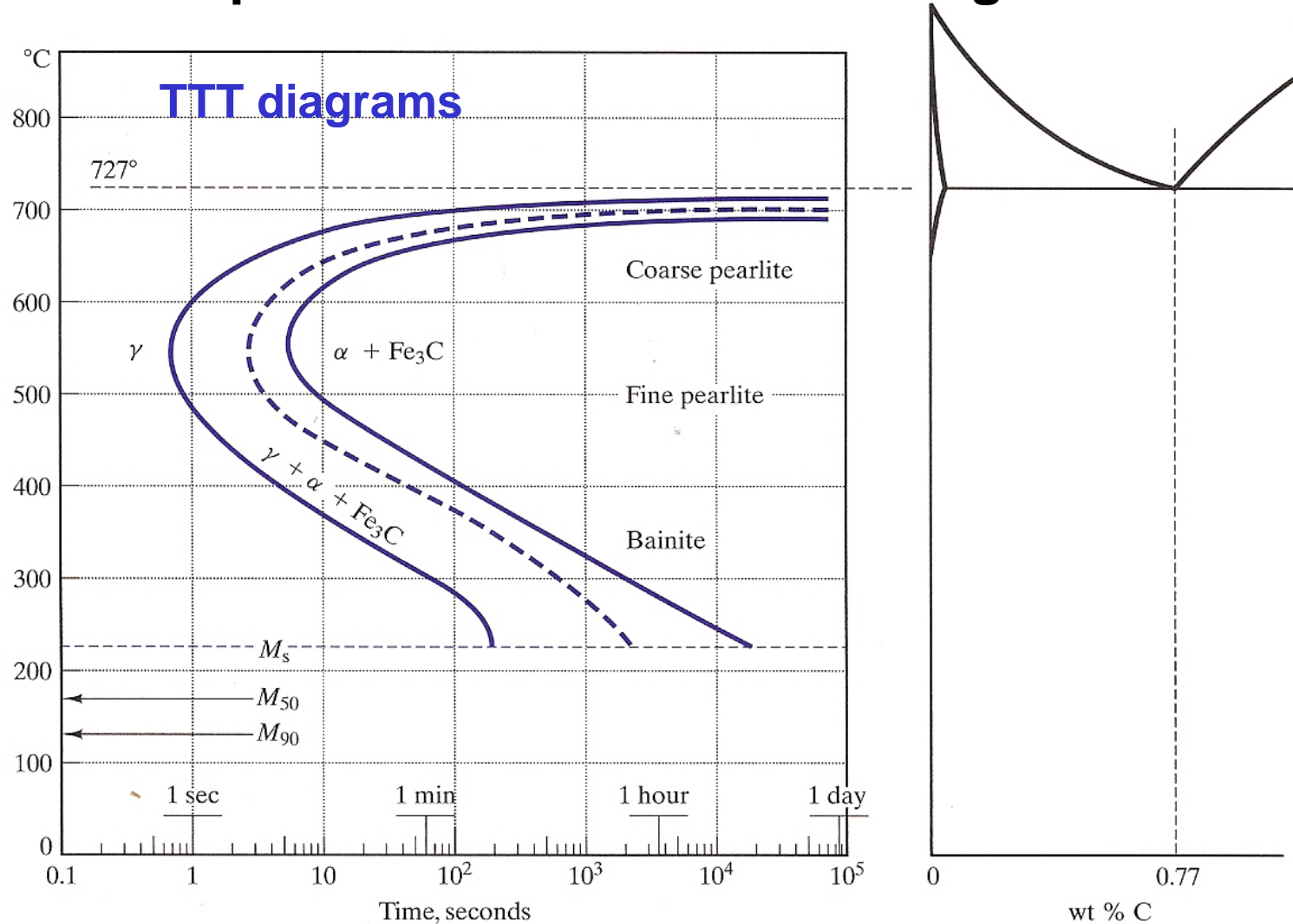


**FIGURE 10.11** A more complete TTT diagram for eutectoid steel than was given in Figure 10.7. The various stages of the time-independent (or diffusionless) martensitic transformation are shown as horizontal lines.  $M_s$  represents the start,  $M_{50}$  represents 50% transformation, and  $M_{90}$  represents 90% transformation. One hundred percent transformation to martensite is not complete until a final temperature ( $M_f$ ) of  $-46^\circ\text{C}$ .

# \* Continuous Cooling Transformation diagrams

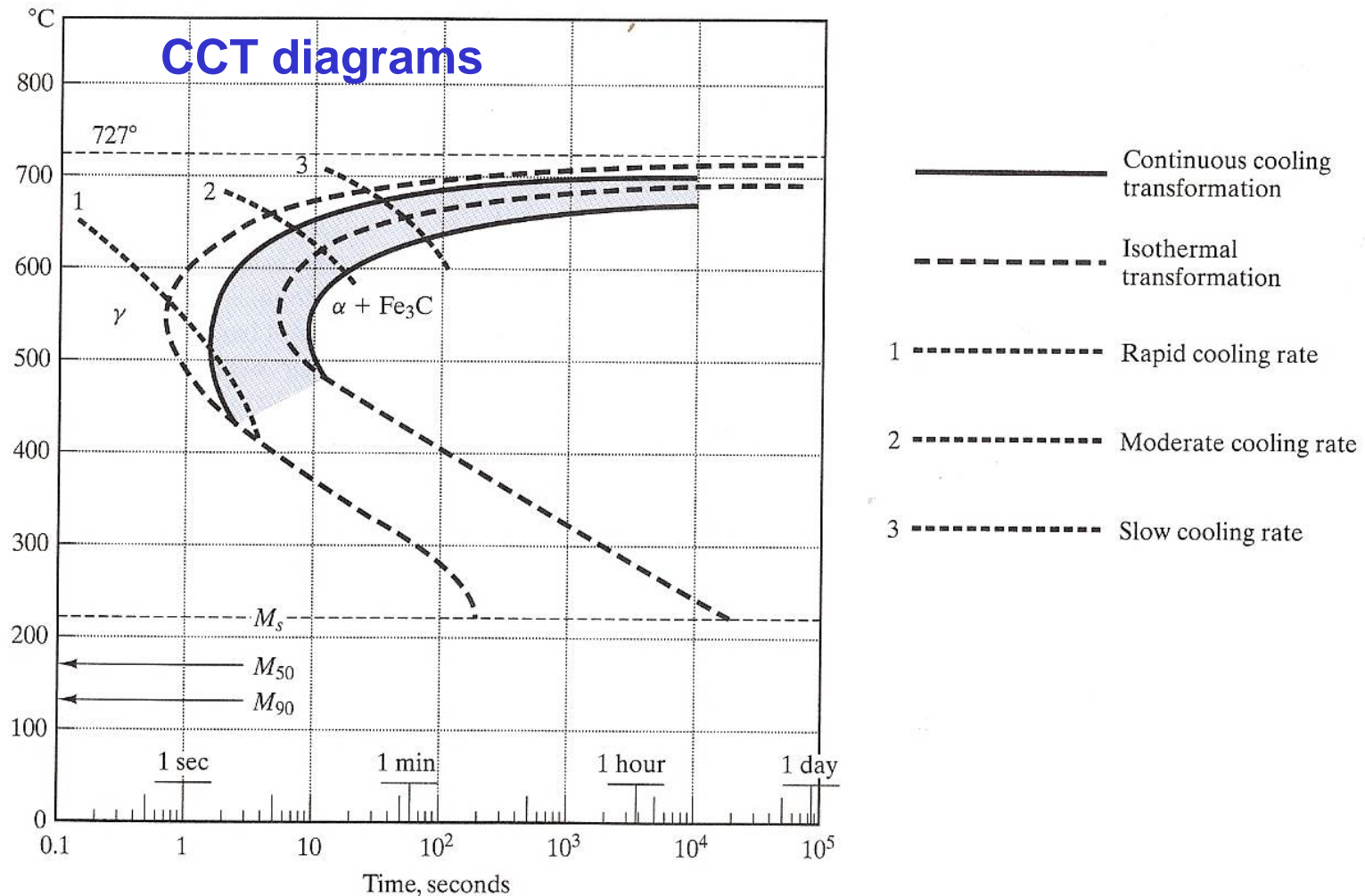


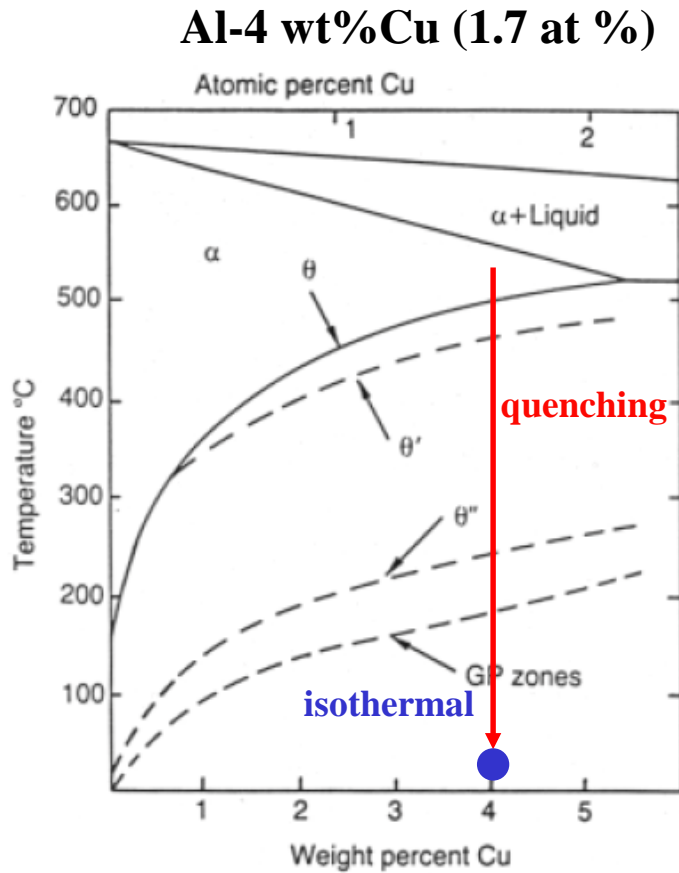
**FIGURE 10.14** A continuous cooling transformation (CCT) diagram is shown superimposed on the isothermal transformation diagram of Figure 10.11. The general effect of continuous cooling is to shift the transformation curves downward and toward the right. (After Atlas of Isothermal Transformation and Cooling Transformation Diagrams, American Society for Metals, Metals Park, OH, 1977.)



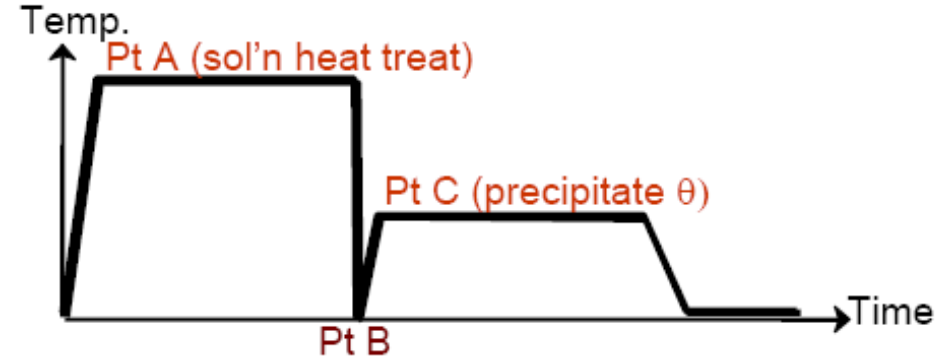
Let us now turn to a consideration of some examples of the great variety of civilian transformations in solid.

## 5.5 Precipitation in Age-Hardening Alloys

### Precipitation in Aluminum-Copper Alloys



$\alpha_0$  540°C heat treatment →  
 Quenching + Isothermal (below 180°C)  
 Supersaturated solid solution



→  $\alpha_1$ +GP zones

→  $\alpha_2$ + $\theta''$  →  $\alpha_3$ + $\theta'$  →  $\alpha_4$ + $\theta$

(CuAl<sub>2</sub>)

Fig. 5.25 Al-Cu phase diagram showing the metastable GP zone,  $\theta''$  and  $\theta'$  solvuses. (Reproduced from G. Lorimer, *Precipitation Processes in Solids*, K.C. Russell and H.I. Aaronson (Eds.), The Metallurgical Society of AMIE, 1978, p. 87.)

In most system,  $\alpha$ ,  $\beta$  phase~ different crystal structure → incoherent nuclei with large  $\gamma$  ~ impossible to homogeneous nucleation of  $\beta$  → Homogeneous nucleation of metastable phase  $\beta'$  (GP Zones, Section 5.5.1)

## Transition phases

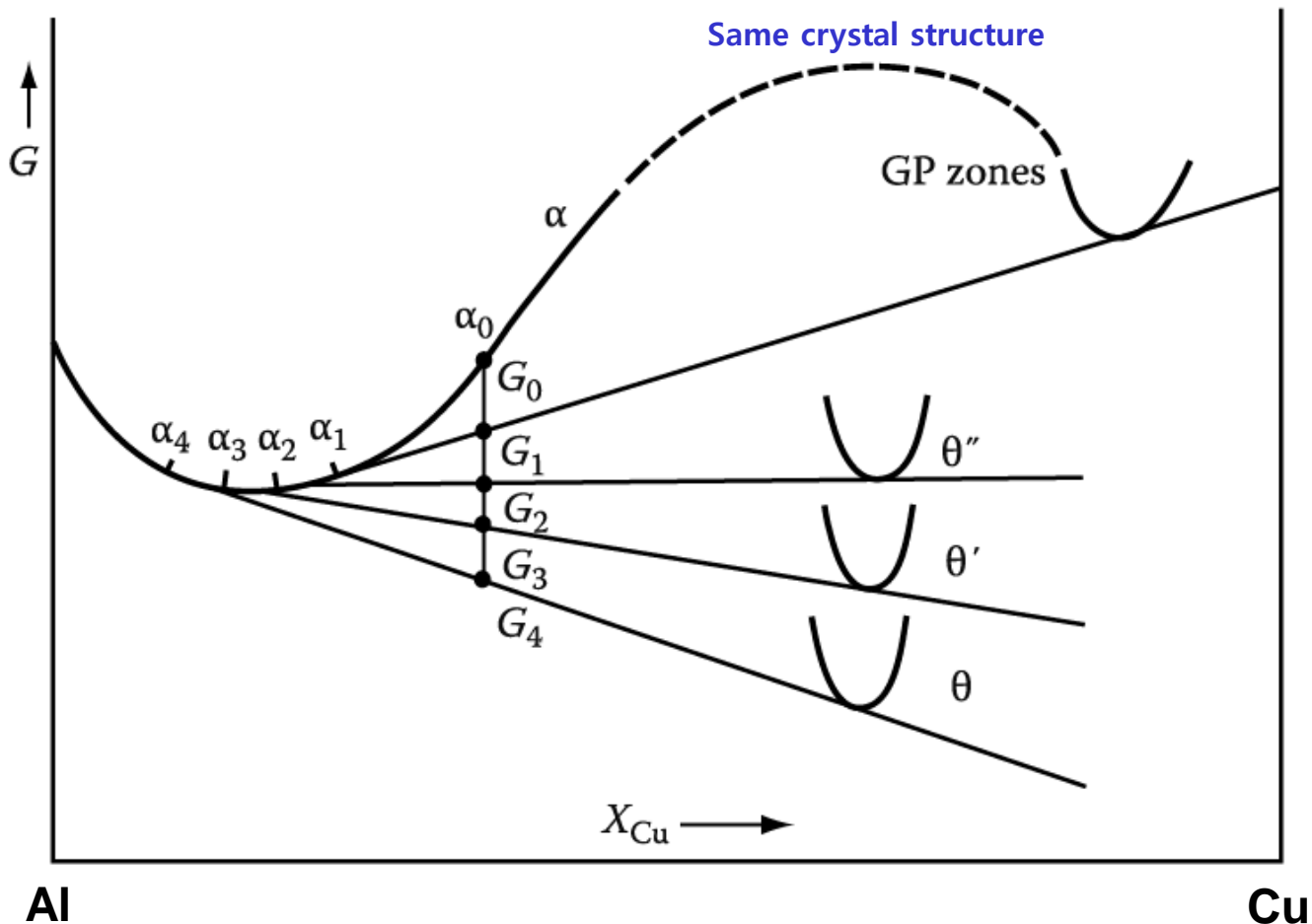
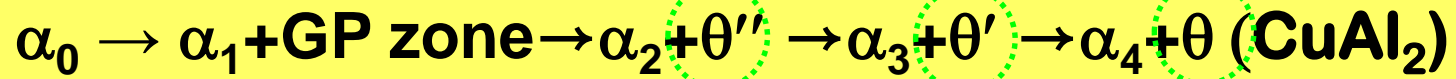


Fig. 5.27 A schematic molar free energy diagram for the Al-Cu system.

# \* Effect of Aging Temperature on the Sequence of Precipitates

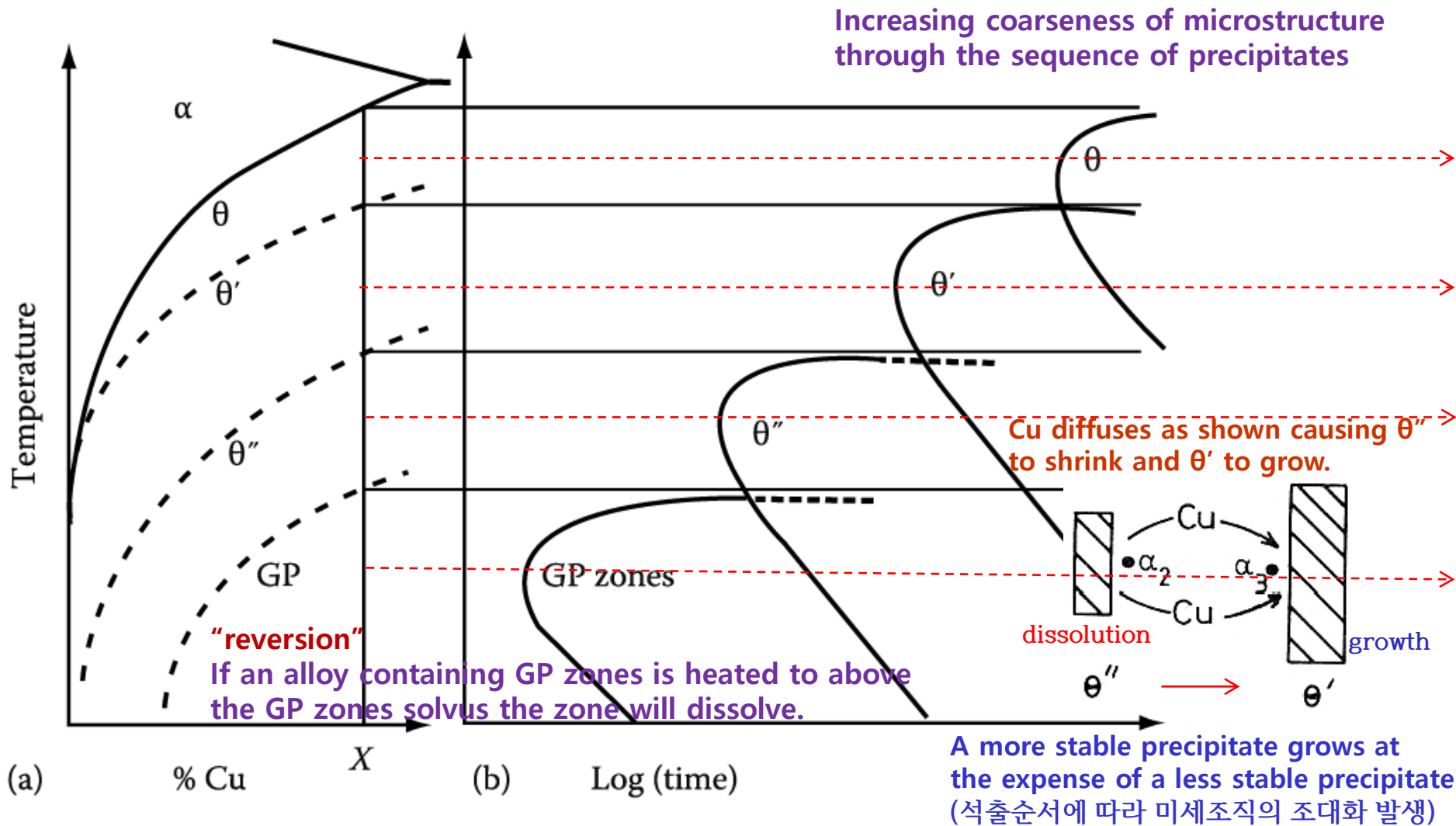


Fig. 5.32 (a) Metastable solvus lines in Al-Cu (schematic).

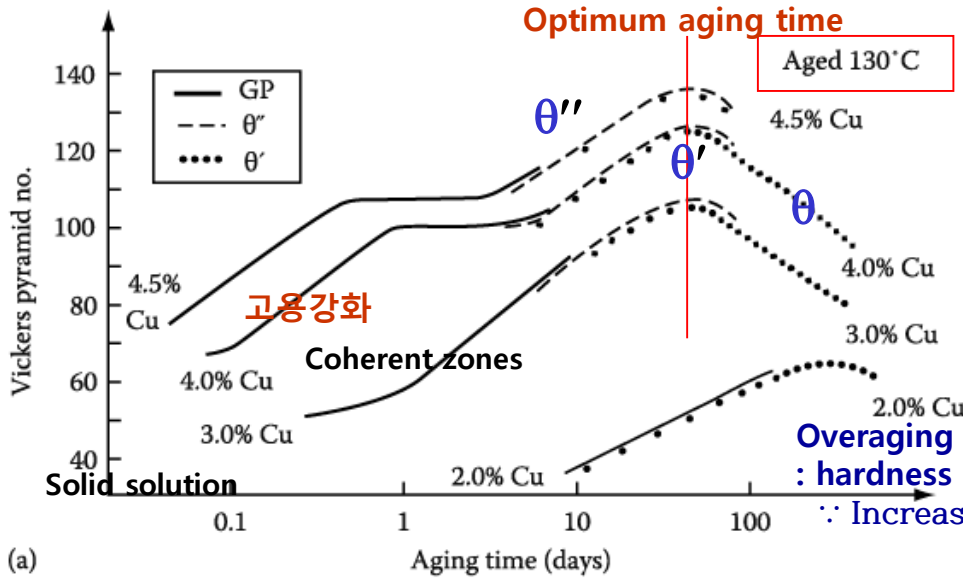
(b) Time for start of precipitation at different temperatures for alloy X in (a).

# 5.5.4. Age Hardening

Transition phase precipitation → great improvement in the mechanical properties

Coherent precipitates → highly strained matrix → the main resistance to the  $\odot$  movement: solid solution hardening

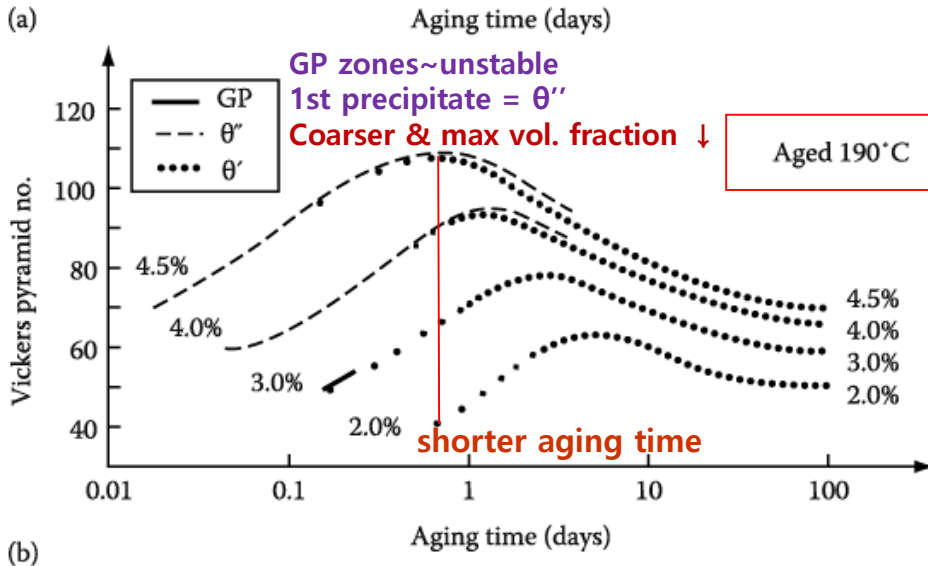
## Hardness vs. Time by Ageing



Maximum hardness ~ largest fraction of  $\theta''$   
(coherent precipitates)

Ageing at 130°C produces higher maximum hardness than ageing at 190°C.

At 130°C, however, it takes too a long time (several tens of days).



How can you get the high hardness for the relatively short ageing time (up to 24h)?

**Double ageing treatment**  
first below the GP zone solvus → fine dispersion of GP zones then ageing at higher T.

: Engineering alloys are not heat treated for max. strength alone. → to optimize other properties  
**best heat treatment in practice**

Fig. 5. 37 Hardness vs. time for various Al-Cu alloys at (a) 130 °C (b) 190 °C

# Contents for today's class

## < Phase Transformation in Solids >

### 1) Diffusional Transformation

Long range diffusion

#### (a) Precipitation

Q4: How can you design an alloy with high strength at high T?

Q5: Quenched-in vacancies vs Precipitate-free zone

Q6: Spinodal Decomposition

Q7: Precipitation of Ferrite from Austenite ( $\gamma \rightarrow \alpha$ )

#### (b) Eutectoid Transformation (5.8 절)

---

Short range diffusion

(c) Order-disorder Transformation (1.3.7 절)

(d) Massive Transformation (5.9 절)

(e) Polymorphic Transformation

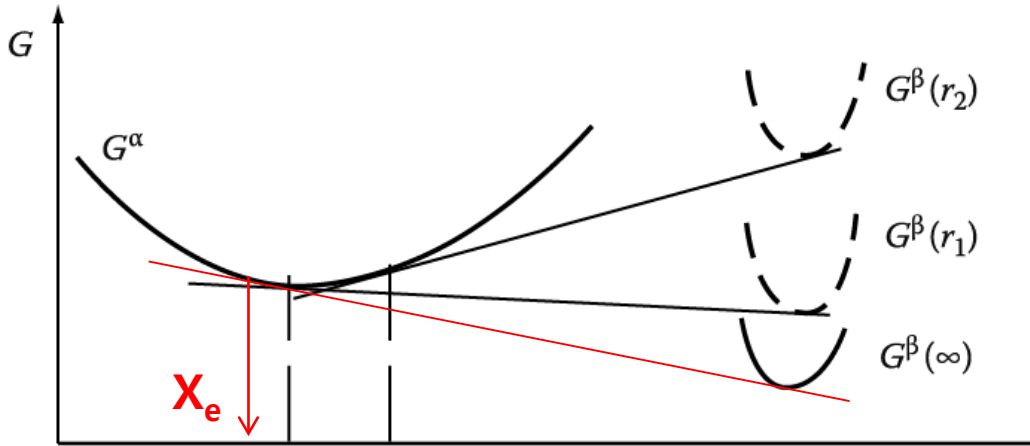
**Q4: How can you design an alloy  
with high strength at high T?**

Microstructure of a two phase alloy is always unstable if the total interfacial free E is not a minimum. →

## 5.5.6. Particle Coarsening (smaller total interfacial area → loss of strength or disappearance of GB pinning effect → particular concern in the design of materials for high temp. applications)

### Two Adjacent Spherical Precipitates with Different Diameters

(Gibbs-Thomson effect: radius of curvature ↓ →  $X_B$  ↑) Assumption: volume diffusion is the rate controlling factor



$$(\bar{r})^3 - r_0^3 = kt$$

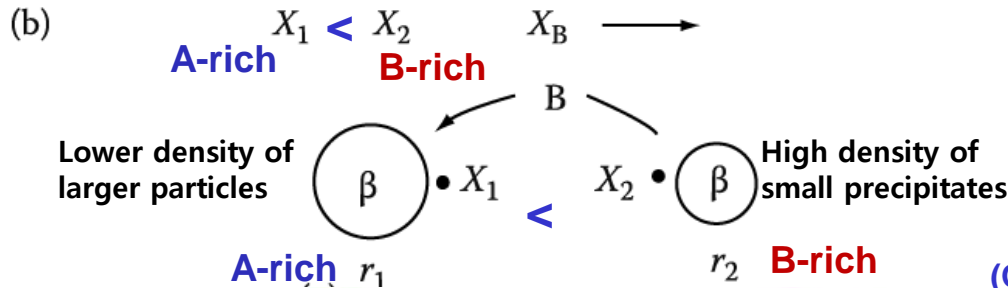
Average radius

where  $k \propto D\gamma X_e$

( $X_e$ : Equil. solubility of very large particles)

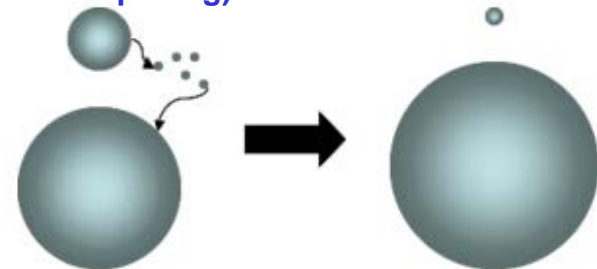
Coarsening rate

$$\frac{d\bar{r}}{dt} \propto \frac{k}{\bar{r}^2}$$



$D$  and  $X_e \sim \exp(-Q/RT)$   
 $\bar{r}$  Rapidly increase with Increasing temp. ⇒ CR ↑

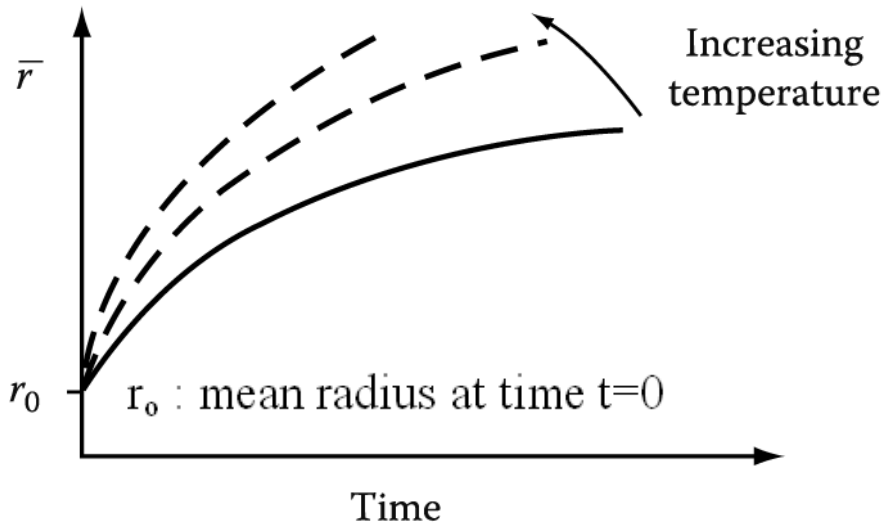
(Ostwald Ripening)



: Concentration gradient in matrix → diffusion → small particle\_shrink/ large particle\_grow

## 5.5.6. Particle Coarsening

### The Rate of Coarsening with Increasing Time and Temp.



$\bar{r}$  ~ Particular concern in the design of materials for high temperature applications

Undesirable degradation of properties:  
less strength/ disappearance of GB pinning effects

How can you design an alloy with high strength at high T?

→ fine precipitate dispersion

hint)  $\frac{d\bar{r}}{dt} \propto \frac{k}{\bar{r}^2}$       $k \propto D\gamma X_e$

### 1) low $\gamma$

heat-resistant Nimonic alloys

based on Ni-rich Ni-Cr → ordered fcc

$\text{Ni}_3(\text{Ti,Al})$  in Ni-rich matrix → high strength

Ni/ $\gamma'$  interface ~ "fully coherent" ( $10 \sim 30 \text{ mJ m}^{-2}$ )

Maintain a fine structure at high temperature

→ improve creep-rupture life

### 2) low $X_e$ (Oxide ~ very insoluble in metals)

: fine oxide dispersion in a metal matrix

Ex) dispersed fine  $\text{ThO}_2$  (thoria) in W and Ni

→ strengthened for high temperature

### 3) low $D$

Cementite dispersions in tempered steel

→ high  $D$  of carbon → very quickly coarsening

a. substitutional alloying element

→ segregates to carbide → slow coarsening

b. strong carbide-forming elements

→ more stable carbides → lower  $X_e$



## **Q5: Quenched-in vacancies vs Precipitate-free zone**

## 5.5.3. Quenched-in Vacancies

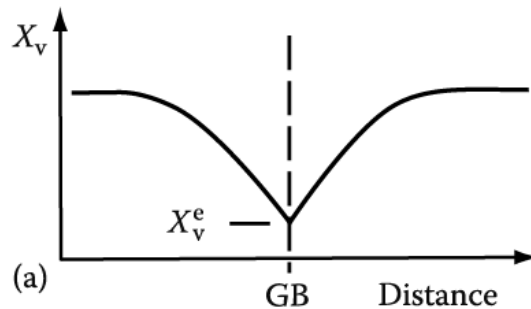
If  $X_v < X_v^c$  critical vacancy supersaturation,  
Precipitate nucleation  $X \rightarrow$  formation of PFZ

In the vicinity of grain boundaries on subsequent aging,

### a) Precipitate-Free Zone (PFZ) due to Vacancy Diffusion during quenching

Solute concentration within the zone  $\sim$  largely unchanged, but no precipitate at GB  
 $\therefore$  a critical vacancy supersaturation must be exceeded for nucleation to occur.

- a) Excess  $\nabla \rightarrow \textcircled{\text{D}}$  nucleation and moving  $\uparrow$ :  
Heterogeneous nucleation sites  $\uparrow$
- b) Excess  $\nabla \rightarrow$  atomic mobility  $\uparrow$  at ageing temp:  
speeds up the process of nucleation and growth
- ex) rapid formation of GP zones at the relatively low  
ageing temperature. (possible to RT aging in Al-Cu alloy)



Similar PFZs can also form at inclusions and dislocations.

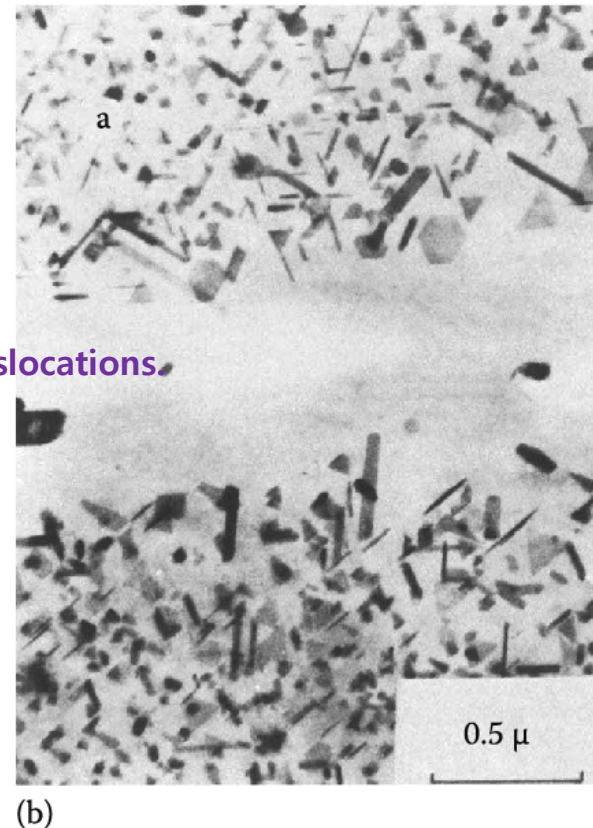
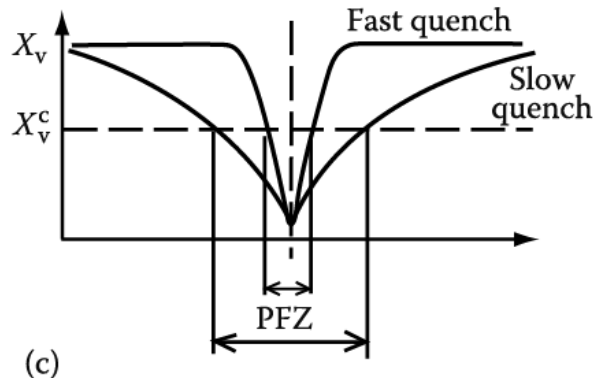


Fig. 5.35 A PFZ due to vacancy diffusion to a grain boundary during quenching.

(a) Vacancy concentration profile. (b) A PFZ in an Al-Ge alloy (x 20,000)

(c) Dependence of PFZ width on critical vacancy concentration  $X_v^c$  and rate of quenching.

## \* Equilibrium Vacancy Concentration

at equilibrium  $\left( \frac{dG}{dX_V} \right)_{X_V = X_V^e} = 0$

$$\Delta H_V - T\Delta S_V + RT \ln X_V^e = 0$$

A constant  $\sim 3$ , independent of T

Rapidly increases with increasing T

$$X_V^e = \exp \frac{\Delta S_V}{R} \exp \frac{-\Delta H_V}{RT}$$

putting  $\Delta G_V = \Delta H_V - T\Delta S_V$

$$X_V^e = \exp \frac{-\Delta G_V}{RT}$$

increases exponentially with increasing T

- In practice,  $\Delta H_V$  is of the order of 1 eV per atom and  $X_V^e$  reaches a value of about  $10^{-4} \sim 10^{-3}$  at the melting point of the solid

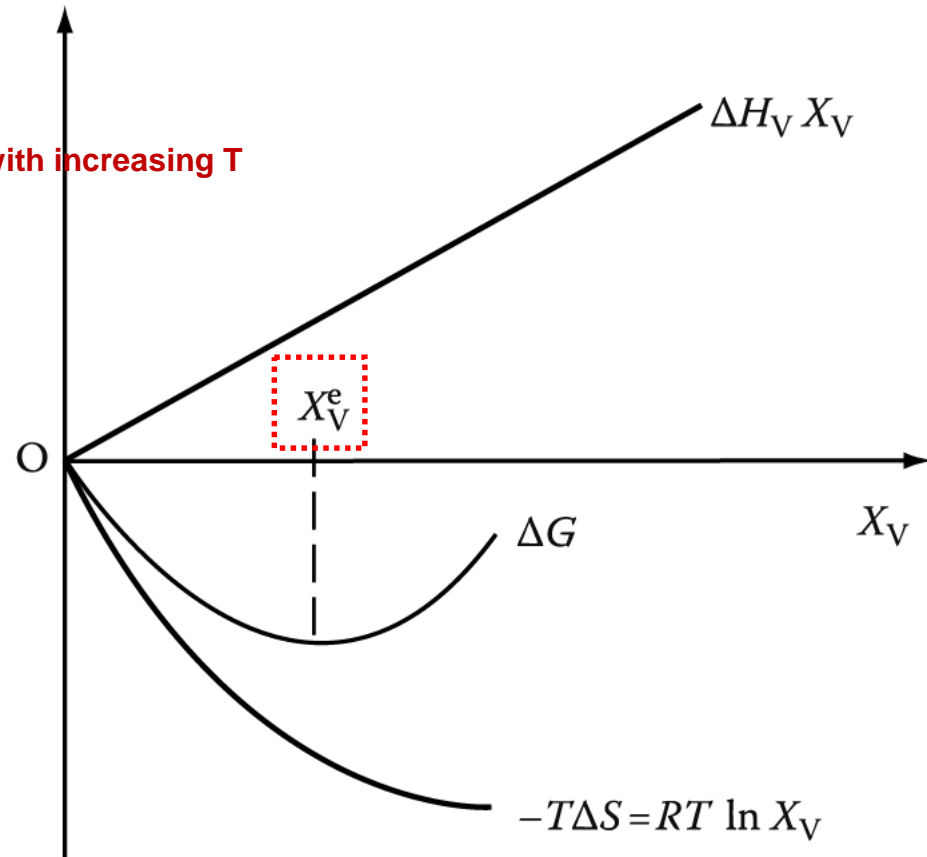


Fig. 1.37 Equilibrium vacancy concentration.

: adjust so as to reduce G to a minimum

b) Another cause of PFZs can be **the nucleation and growth of GB precipitates** during cooling from the solution treatment temperature.

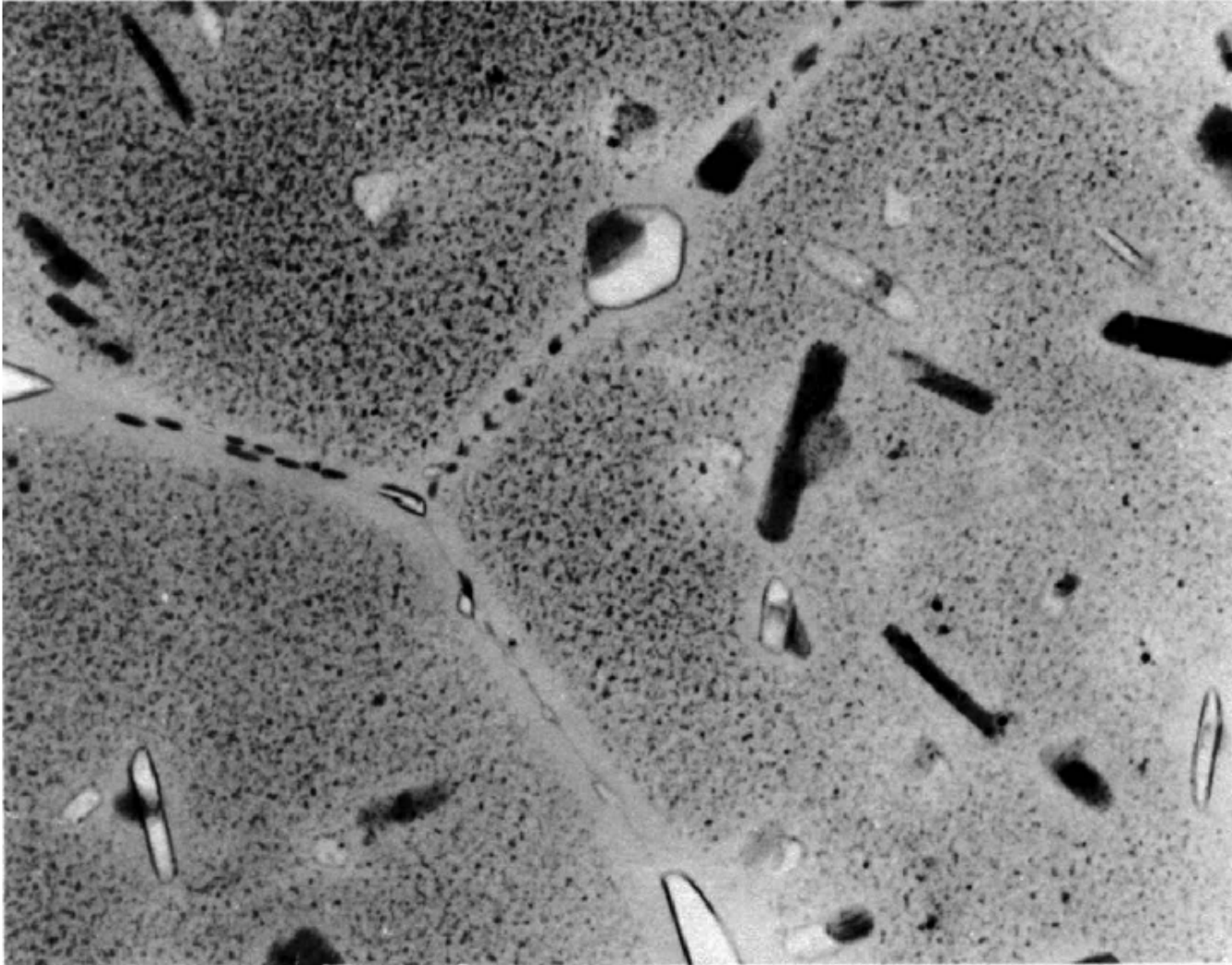


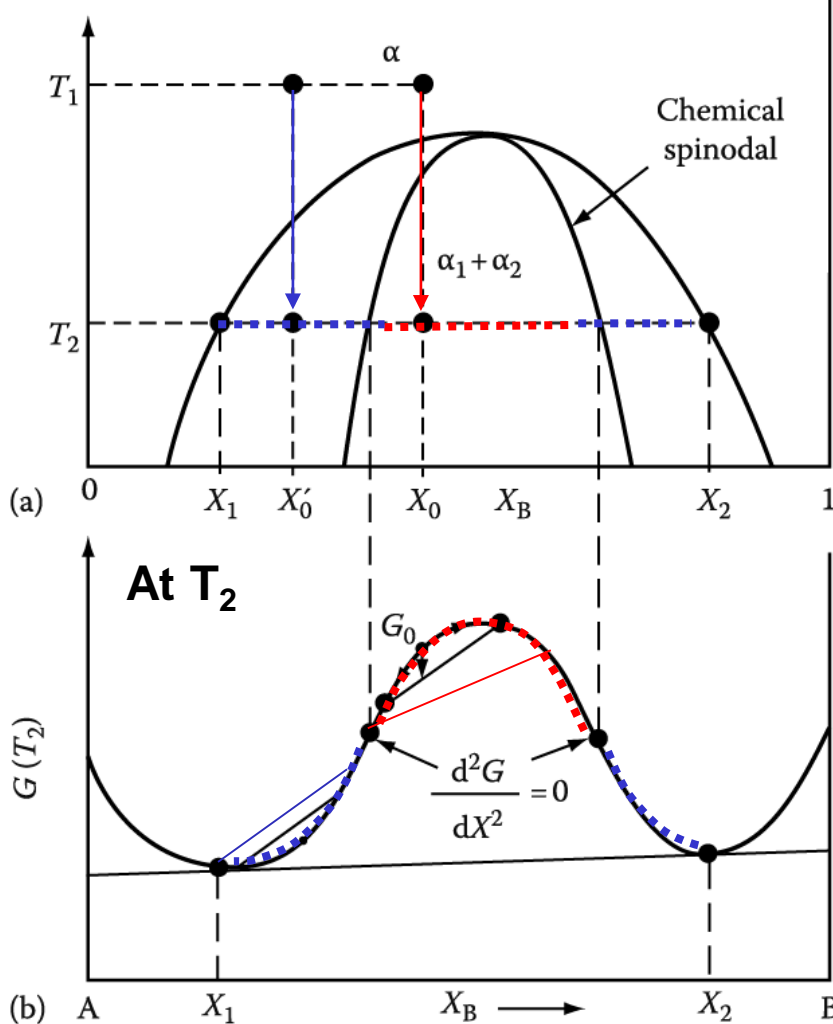
Fig. 5.36 PFZs around grain boundaries in a high-strength commercial Al-Zn-Mg-Cu alloy. 20  
Precipitates on grain boundaries have extracted solute from surrounding matrix. (x 59,200)

## **Q6: Spinodal Decomposition**

# 5.5.5 Spinodal Decomposition

## Spinodal mode of transformation has no barrier to nucleation

: describing the transformation of a system of two or more components in a metastable phase into two stable phases



How does it differ between **inside** and **outside the inflection point** of Gibbs free energy curve?

1) **Within the spinodal**  $\frac{d^2G}{dX^2} < 0$

: phase separation by small fluctuations in composition/  
"up-hill diffusion"

2) If the alloy lies **outside the spinodal**, small variation in composition leads to an increase in free energy and the alloy is therefore **metastable**.

The free energy can only be decreased if nuclei are formed with a composition very different from the matrix.

→ **nucleation and growth**  
: "down-hill diffusion"

Fig. 5.38 Alloys between the spinodal points are unstable and can decompose into two coherent phases  $\alpha_1$  and  $\alpha_2$  without overcoming an activation energy barrier. Alloys between the coherent miscibility gaps and the spinodal are metastable and can decompose only after nucleation of the other phase.

**a) Composition fluctuations within the spinodal**

**b) Normal down-hill diffusion outside the spinodal**

**up-hill diffusion**

**down-hill diffusion**

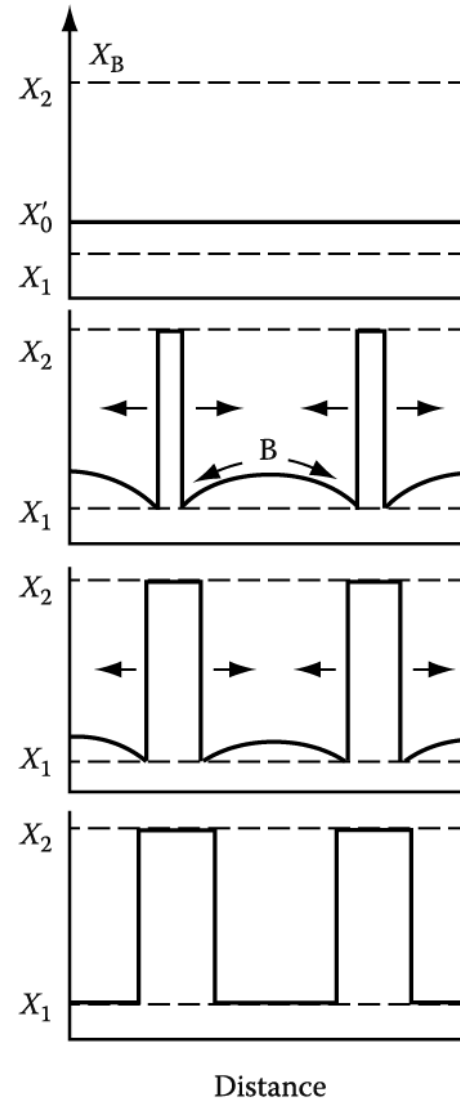
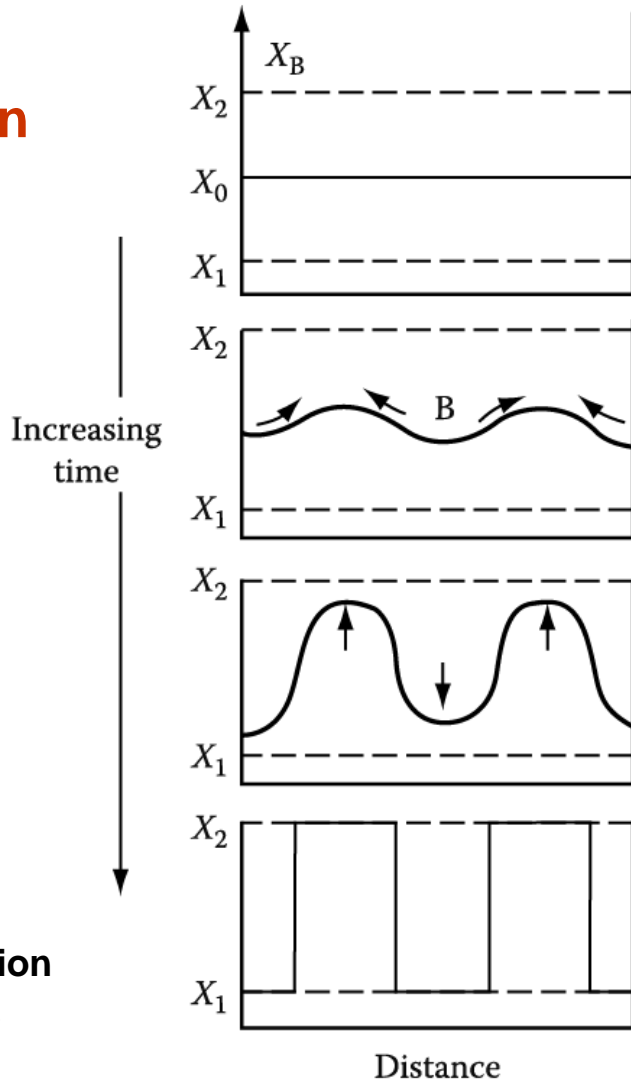
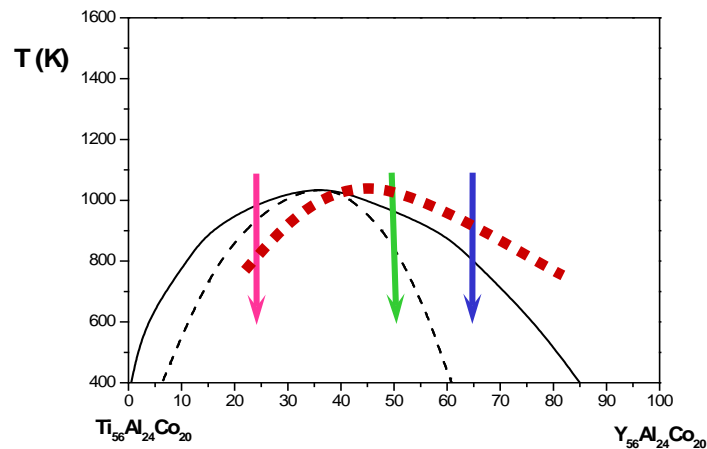
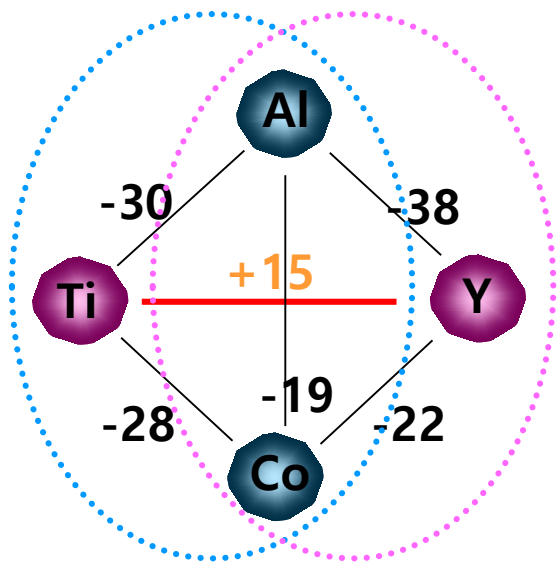


Fig. 5.39 & 5.40 schematic composition profiles at increasing times in (a) an alloy quenched into the spinodal region ( $X_0$  in Figure 5.38) and (b) an alloy outside the spinodal points ( $X'_0$  in Figure 5.38)

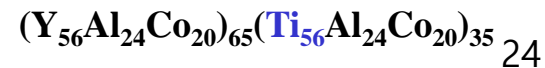
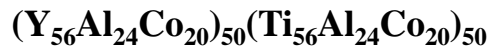
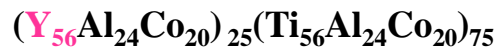
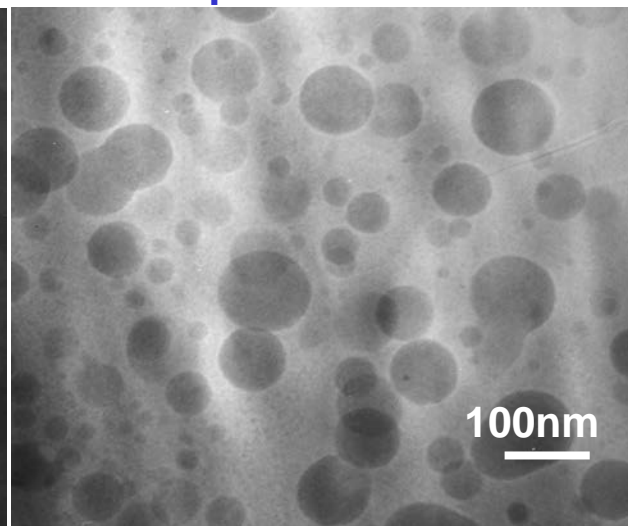
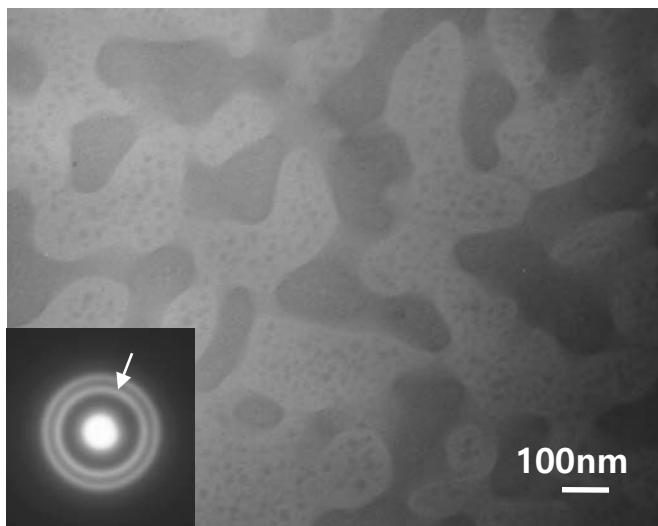
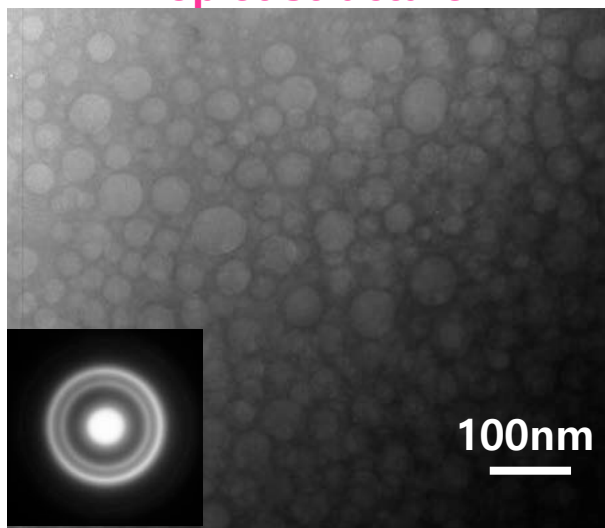
# Phase separation



Droplet structure

Interconnected structure

Droplet structure





## 5.5.5 Spinodal Decomposition

### \* The Rate of Spinodal decomposition

#### a) Rate controlled by interdiffusion coefficient $D$ (상호확산계수)

Within the spinodal,

composition fluctuation  
(next page)

$$\propto \exp(-t / \tau)$$

$$\tau = -\lambda^2 / 4\pi^2 D$$

$\tau$ : characteristic time constant  
 $\lambda$ : wavelength of the composition modulations  
(assumed one-dimensional)

b) Kinetics depends on  $\lambda$ : Transformation rate  $\uparrow$  as  $\lambda \downarrow$  (as small as possible).

But, minimum value of  $\lambda$  below which spinodal decomposition cannot occur.

# Solutions to the diffusion equations

## Ex1. **Homogenization** of sinusoidal varying composition in the **elimination of segregation in casting**

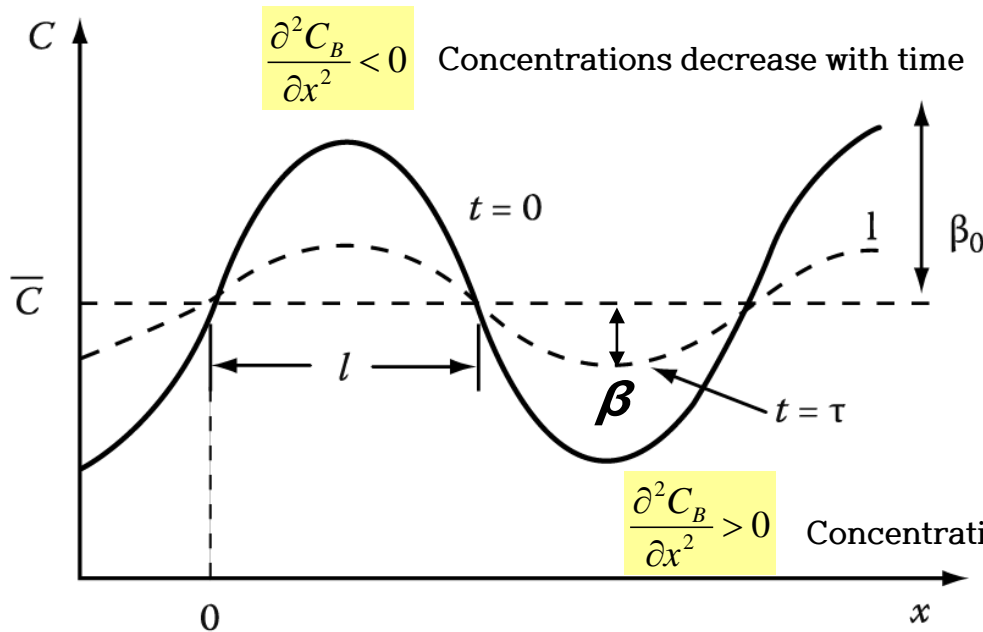


Fig. 2.10 The effect of diffusion on a sinusoidal variation of composition.

$$C = \bar{C} + \beta_0 \sin \frac{\pi x}{l} \quad \text{at } t=0$$

$$C = \bar{C} + \beta_0 \sin \frac{\pi x}{l} \exp\left(\frac{-t}{\tau}\right)$$

$$\beta = \beta_0 \exp(-t/\tau) \quad \text{at } x = \frac{l}{2}$$

Amplitude of the concentration profile ( $\beta$ ) decreases exponentially with time,  $C \rightarrow \bar{C}$

$$\tau = \frac{l^2}{\pi^2 D} \quad \tau : \text{relaxation time}$$

**"decide homogenization rate"**

The initial concentration profile will not usually be sinusoidal, but in general any concentration profile can be considered as the sum of an infinite series of sine waves of varying wavelength and amplitude, and each wave decays at a rate determined by its own " $\tau$ ". Thus, the short wavelength terms die away very rapidly and the homogenization will ultimately be determined by  $\tau$  for the longest wavelength component.

## 5.5.5 Spinodal Decomposition

### \* The Rate of Spinodal decomposition

#### a) Rate controlled by interdiffusion coefficient $D$ (상호확산계수)

Within the spinodal,

composition fluctuation  $\propto \exp(-t / \tau)$   
(next page)

$$\tau = -\lambda^2 / 4\pi^2 D$$

$\tau$ : characteristic time constant  
 $\lambda$ : wavelength of the composition modulations  
(assumed one-dimensional)

#### b) Kinetics depends on $\lambda$ : Transformation rate $\uparrow$ as $\lambda \downarrow$ (as small as possible).

But, minimum value of  $\lambda$  below which spinodal decomposition cannot occur.

\* Calculation of the wavelength ( $\lambda$ ) of the composition fluctuations

→ Free Energy change for the decomposition

1) Decomposition of  $X_0$  into  $X_0 + \Delta X$  and  $X_0 - \Delta X$

What would be an additional energy affecting spinodal decomposition?

In practice, it is necessary to consider two important factors

2) interfacial energy

3) coherency strain energy

1) Decomposition of  $X_0$  into  $X_0 + \Delta X$  and  $X_0 - \Delta X$

$$\Delta G_{chem} = \frac{1}{2} \frac{d^2G}{dX^2} (\Delta X)^2$$

Gibb's free energy reduction by compositional change

$$f(a+h) = f(a) + f'(a)h + \frac{f''(a)}{2!} h^2 + \dots$$

$$\left[ \begin{aligned} G(X_0 + \Delta X) &\approx G(X_0) + G'(X_0)\Delta X + \frac{G''(X_0)}{2!} \Delta X^2 \\ G(X_0 - \Delta X) &\approx G(X_0) - G'(X_0)\Delta X + \frac{G''(X_0)}{2!} \Delta X^2 \end{aligned} \right.$$

$$\Delta G_{chem} = \frac{G(X_0 + \Delta X) + G(X_0 - \Delta X)}{2} - G(X_0)$$

$$= \frac{G''(X_0)}{2!} \Delta X^2 = \frac{1}{2} \frac{d^2G}{dX^2} \Delta X^2$$

# 5.5.5 Spinodal Decomposition

2) During the early stages, the interface between A-rich and B-rich region is not sharp but very diffuse. → **diffuse interface**

$\Delta G$  by formation of interface btw decomposed phases

**Interfacial Energy**  
(gradient energy)

$\propto$  composition gradient across the interface  
: increased # of unlike nearest neighbors in a solution containing composition gradients

$$\Delta G_\gamma = K \left( \frac{\Delta X}{\lambda} \right)^2$$

Max. compositional gradient  $\Delta X/\lambda$

$K$ : a proportionality constant dependent on the difference in the bond energies of like and unlike atom pair

If the size of the atoms making up the solid solution are different, the generation of composition differences,  $\Delta X$  will introduce a **coherency strain energy term,  $\Delta G_s$** .

**3) Coherency Strain Energy**

$$\Delta G_s \propto E \delta^2 \quad \leftarrow \quad \delta = (da/dX) \Delta X / a$$

(atomic size difference)  $\delta$ : misfit between the A-rich & B-rich regions, E: Young's modulus, a: lattice parameter

$$\Delta G_s = \eta^2 (\Delta X)^2 E' V_m$$

$$\text{where } \eta = \frac{1}{a} \left( \frac{da}{dX} \right), E' = E/(1-\nu)$$

$\Delta G_s \sim$  independent of  $\lambda$

$\eta$ : the fractional change in lattice parameter per unit composition change

\* Total free E change by the formation of a composition fluctuation  
1) + 2) + 3)

$$\Delta G = \left\{ \frac{d^2 G}{dX^2} + \frac{2K}{\lambda^2} + 2\eta^2 E' V_m \right\} \frac{(\Delta X)^2}{2}$$

# 5.5.5 Spinodal Decomposition

\* Total free E change by the formation of a composition fluctuation

$$\Delta G = \left\{ \frac{d^2G}{dX^2} + \frac{2K}{\lambda^2} + 2\eta^2 E' V_m \right\} \frac{(\Delta X)^2}{2} < 0$$

## a) Condition for Spinodal Decomposition

(→ a homogeneous solid solution ~ unstable)

$$-\frac{d^2G}{dX^2} > \frac{2K}{\lambda^2} + 2\eta^2 E' V_m$$

## b) The Limit of T and composition in coherent spinodal decomposition

(스피노달 분해가 일어나는 온도와 조성의 한계값)

$$\lambda \rightarrow \infty$$

$$\frac{d^2G}{dX^2} = -2\eta^2 E' V_m$$

→ **coherent spinodal**

It lies entirely within the chemical spinodal ( $d^2G/dX^2=0$ )

( boundary btw ③ & ④, next page )

## Wavelength for coherent spinodal

$$\lambda^2 > -2K / \left( \frac{d^2G}{dX^2} + 2\eta^2 E' V_m \right)$$

→ The minimum possible wavelength ( $\lambda$ ) decreases with increasing undercooling ( $\Delta T \sim \Delta X$ ) below the coherent spinodal.

This figure include the lines defining the equilibrium compositions of the coherent/ incoherent phases that result from spinodal decomposition.

**\* Incoherent(or equilibrium) miscibility gap:  $\Delta H > 0$**

The miscibility gap the normally appears on an equilibrium phase is the incoherent (or equilibrium) miscibility gap. → equilibrium compositions of incoherent phases without strain fields.

a) chemical spinodal:  $d^2G/dX^2=0$ \_no practical importance X

b) Area ② ,  $\Delta G_V - \Delta G_S < 0$  → only incoherent strain-free nuclei can form.

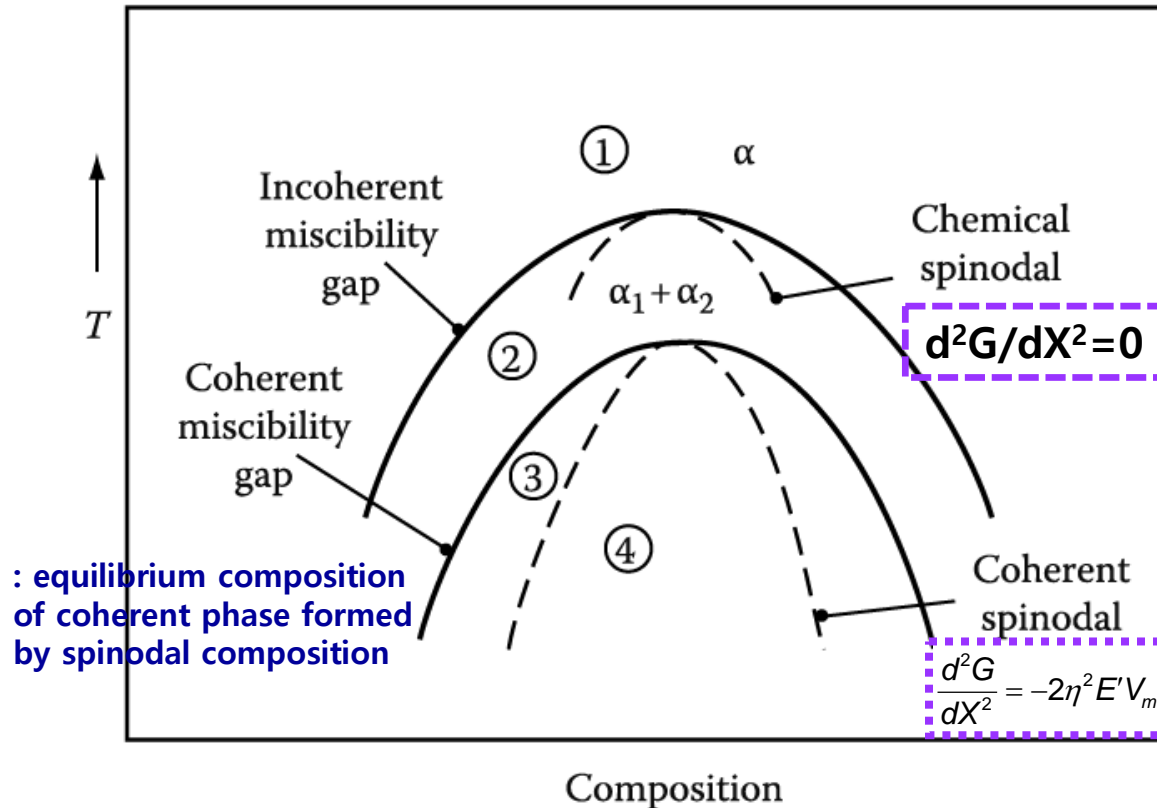


**Figure 5.41 Schematic phase diagram for a clustering system.**

Region 1: homogeneous  $\alpha$  stable. Region 2: homogeneous  $\alpha$  metastable, only incoherent phases can nucleate. Region 3: homogeneous  $\alpha$  metastable, coherent phase can nucleate. Region 4: homogeneous  $\alpha$  unstable, no nucleation barrier, spinodal decomposition occurs.

Spinodal decomposition is not only limited to systems containing a stable miscibility gap

All systems in which GP zones form, for example, containing a metastable coherent miscibility gap, i.e., the GP zone solvus.

→ at high supersaturation, GP zone can form by the spinodal mechanism.

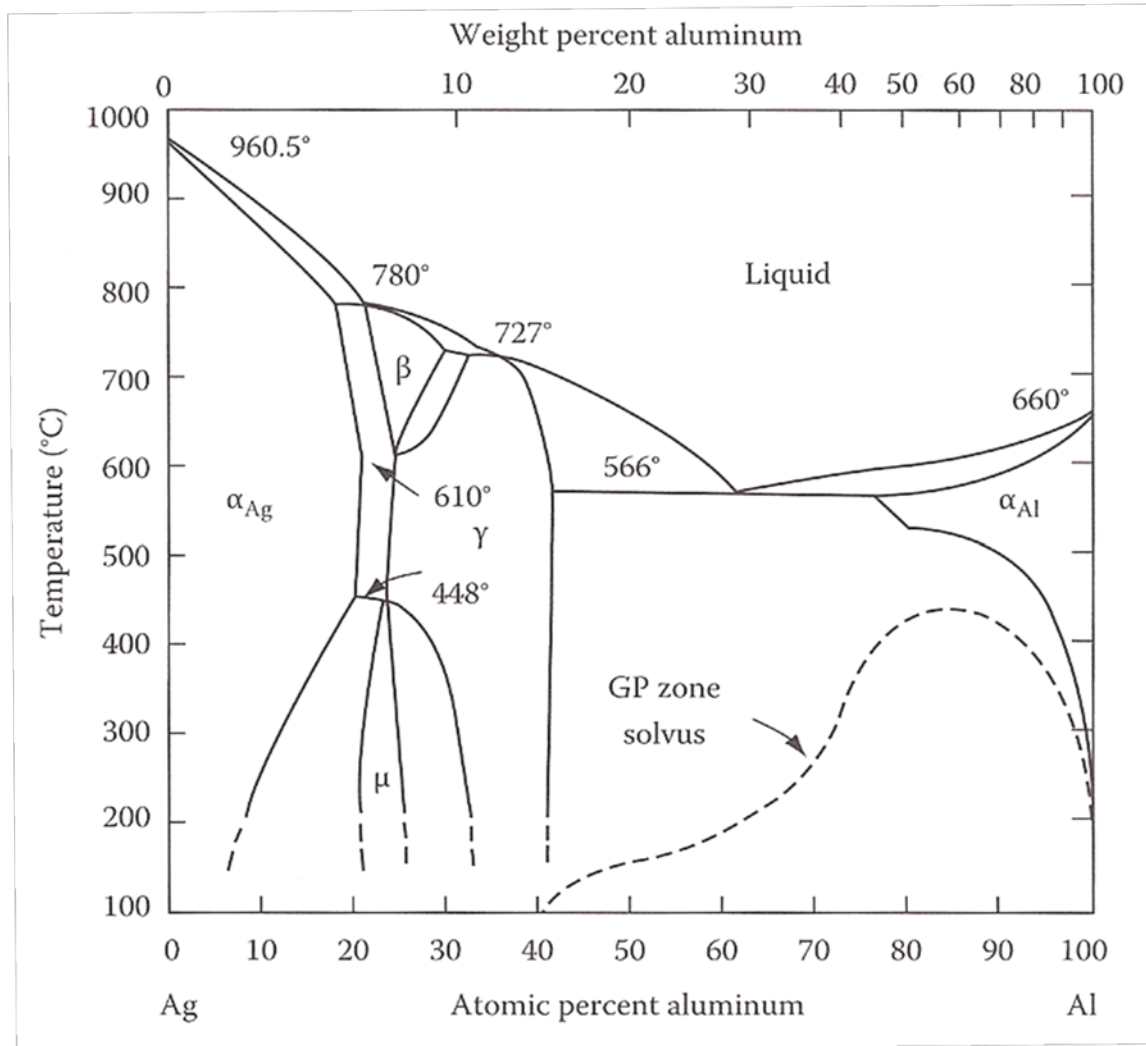


Figure 5.34

Al-Ag phase diagram showing metastable two-phase field corresponding to GP zones.



- The difference in T between the coherent and incoherent miscibility gaps, or the chemical and coherent spinodals  $\propto$  **magnitude of  $|\eta|$**   $\eta$ : the fractional change in lattice parameter per unit composition change
- Large atomic size difference  $\rightarrow$   $|\eta|$  **large**  $\rightarrow$  large undercooling to overcome the strain E effects
- Like Al-Cu, large values of  $|\eta|$  in cubic metals can be mitigated if the misfit strains are accommodated in the elastically soft  $\langle 100 \rangle$  directions.  $\rightarrow$  composition modulations building up normal to  $\{100\}$

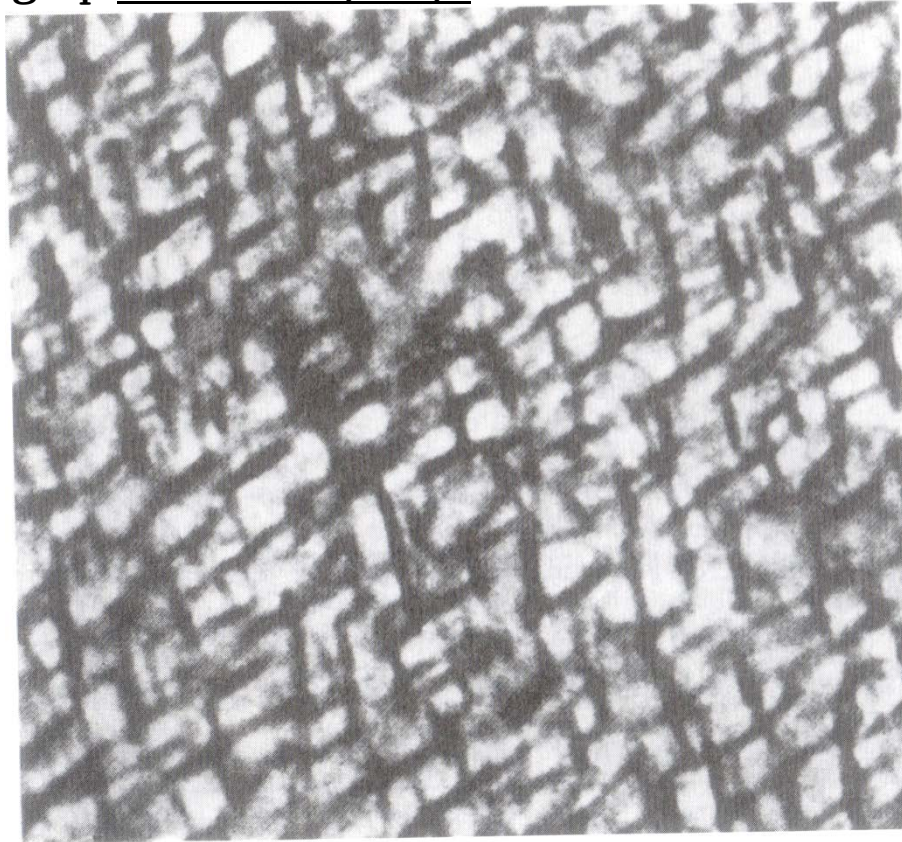


Figure 5.42 A coarsened spinodal microstructure in Al-22.5 Zn-0.1 Mg (at%) solution treated 2h at 400 °C and aged 20h at 100°C. Thin foil electron micrograph.  $\lambda = 25$  nm\_coarsening

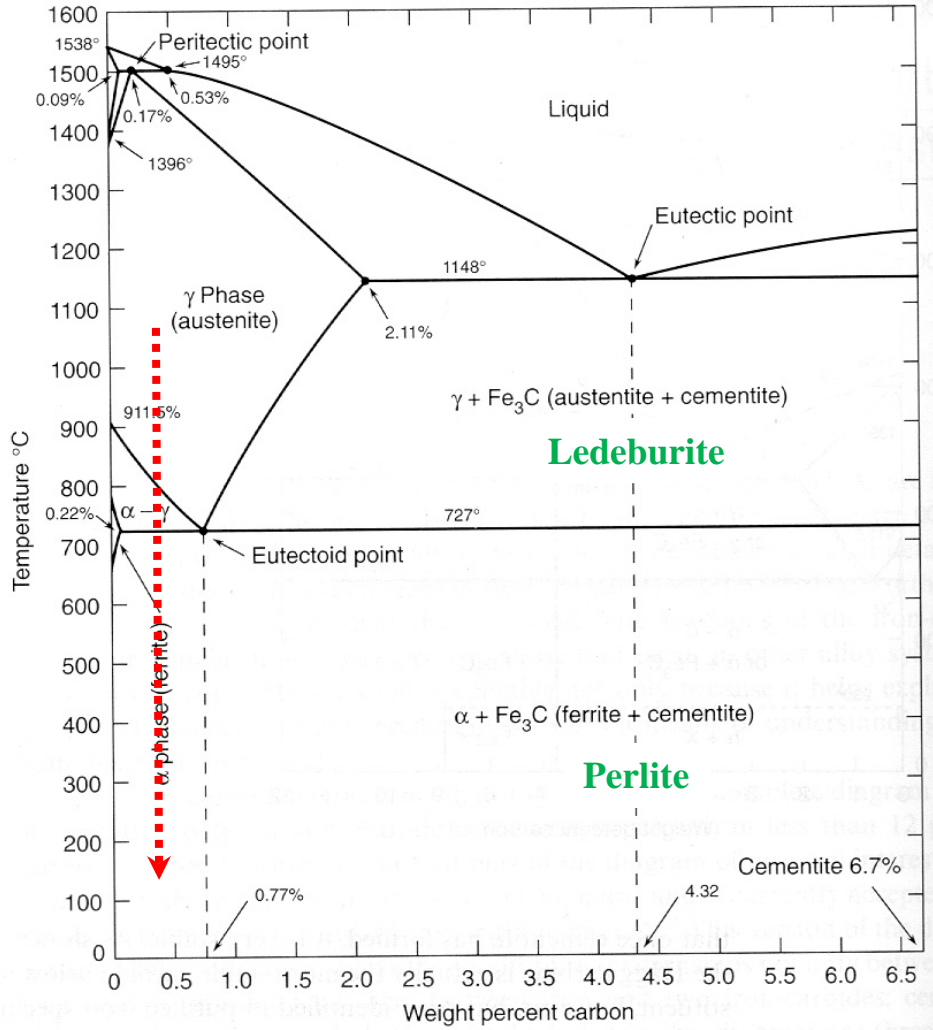
# Q7: Precipitation of Ferrite from Austenite ( $\gamma \rightarrow \alpha$ )

3) Precipitation of equilibrium phase by diffusional transformation

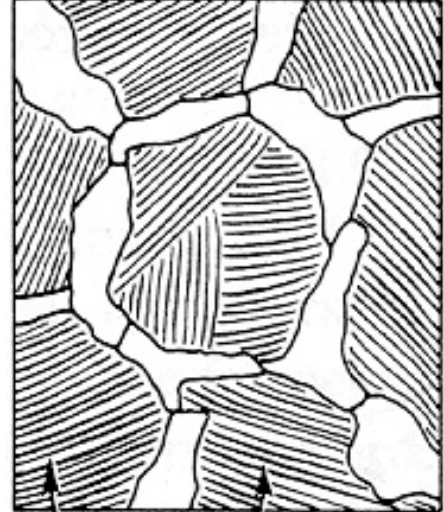
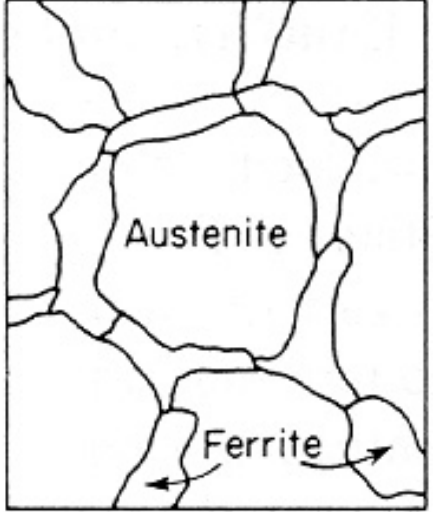
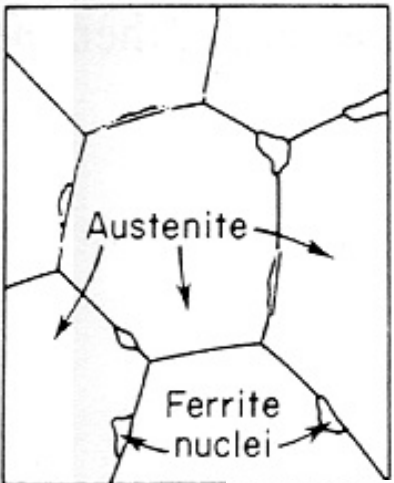
# 5.6. The Precipitation of Ferrite from Austenite ( $\gamma \rightarrow \alpha$ )

(Most important nucleation site: Grain boundary and the surface of inclusions)

## The Iron-Carbon Phase Diagram

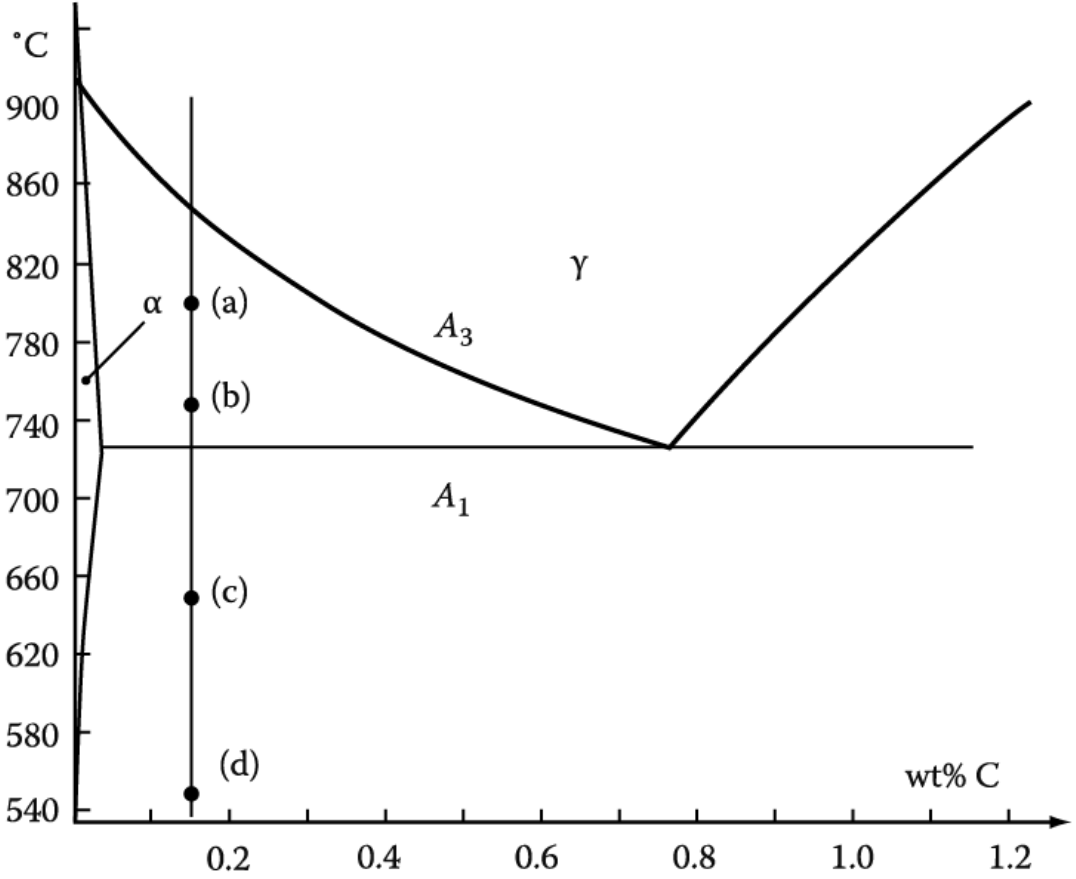


Microstructure (0.4 wt%C) evolved by slow cooling (air, furnace) ?



# 5.6. The Precipitation of Ferrite from Austenite

## Diffusional Transformation of Austenite into Ferrite



**Fe-0.15 wt% C**

After being austenitized, held at  
(a) 800°C for 150 s  
(b) 750°C for 40 s  
(c) 650°C for 9 s  
(d) 550°C for 2 s and then quenched to room T.

**What would be the microstructures?**

Figure 5.45 Holding temperature for steel in Figure. 5.46



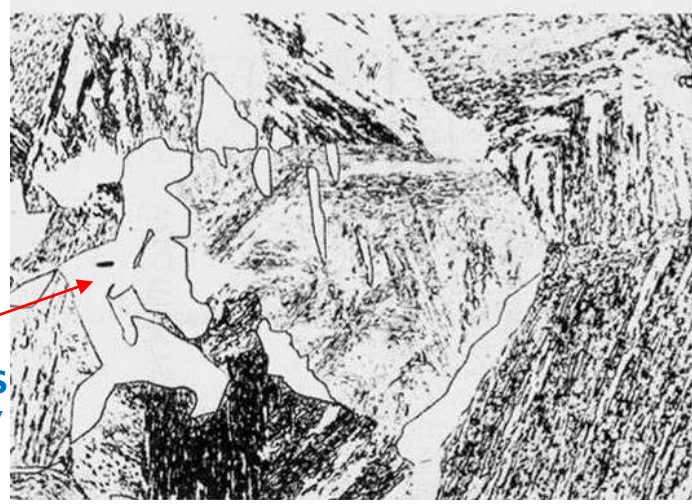
# Microstructures of an austenitized Fe-0.15%C alloy (x 100 except (d), x300)

White:  $\alpha$  ferrite/ Gray: M formed from untransformed  $\gamma$ / fine constituent: a mixture of ferrite and carbide

Primary ferrite allotriomorphs with a few plates  $\Rightarrow$  Many more plates, mostly growing from GBs/ inside  $\alpha$  grain

Smaller  $\Delta T$

(a)  
800°C  
for 150 s

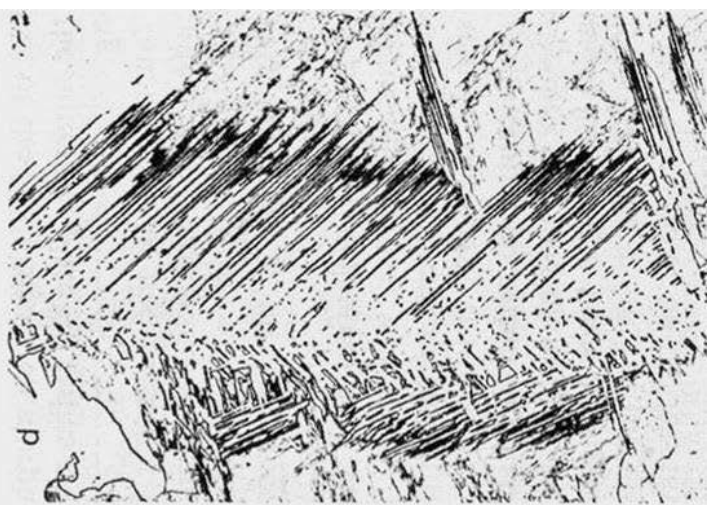


(입계타형) G.B. allotriomorphs  
"blocky" manner/  
Smoothly curved  
& faceted  $\alpha/\gamma$   
Interface are present



(c)  
650°C  
for 9 s

(b)  
750°C  
for 40 s



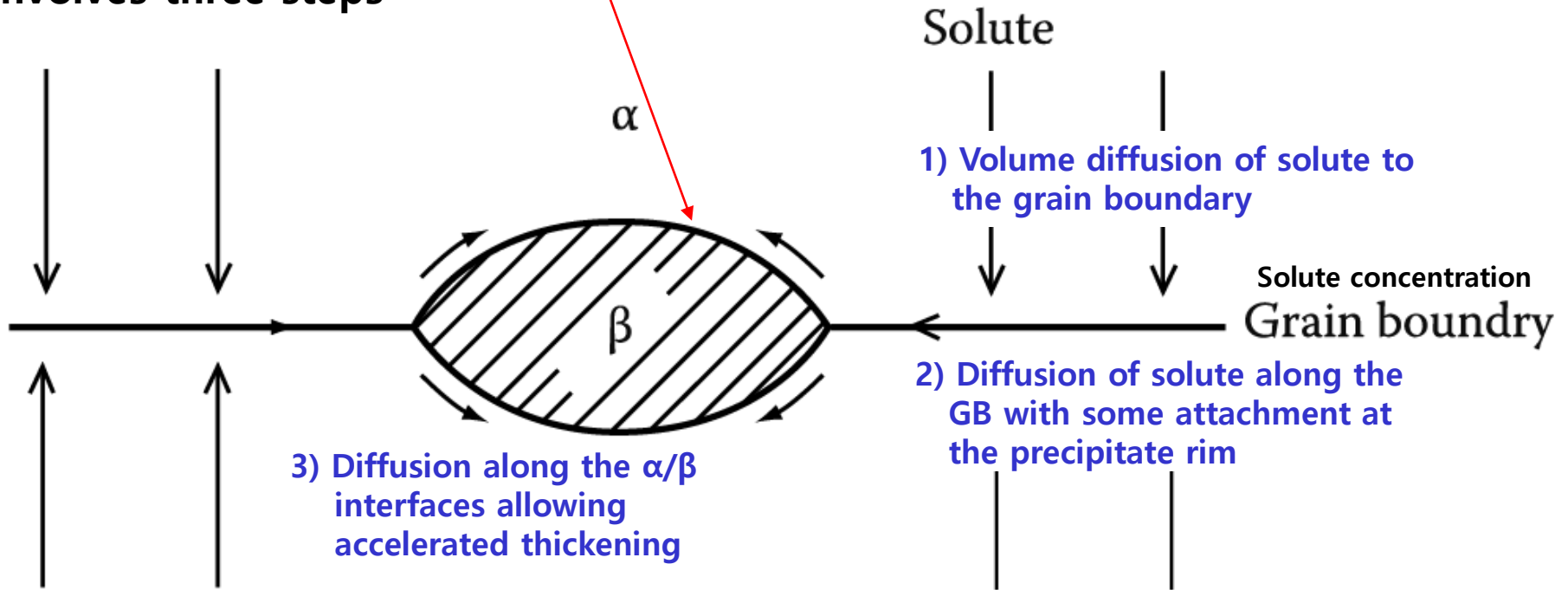
(d)  
550°C  
for 2 s

larger  $\Delta T$

Widmanstätten ferrite side-plates (b), (c), (d) – Finer & faceted coherent interface with increasing "undercooling"

## \* Grain boundary allotriomorph 입계타형

Grain boundary precipitation involves three steps **Faster than allowed by volume diffusion**



치환형 확산이 일어나는 경우 매우 중요/ 침입형 고용체에서는 체적 확산 속도가 크기 때문에 입계나 전위를 통한 단거리 확산은 상대적으로 중요하지 않음.

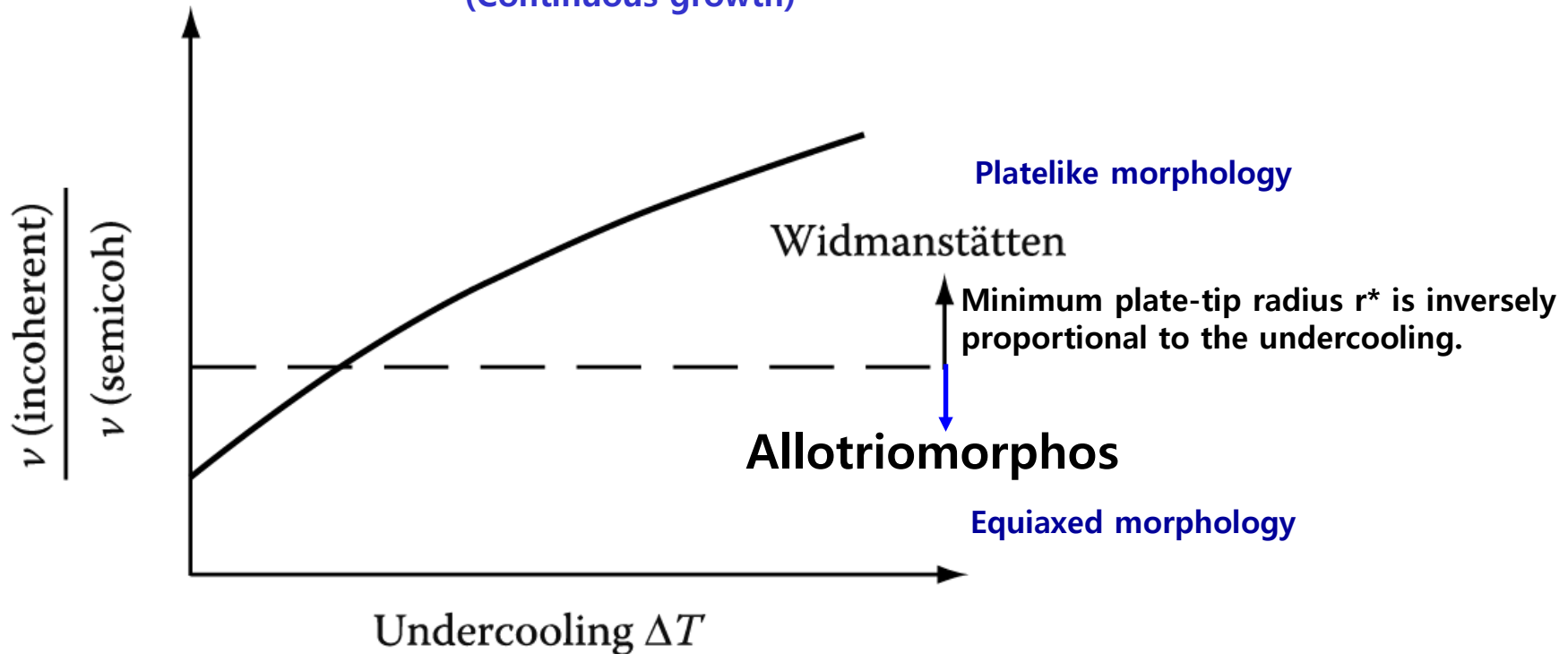
Fig. 5.18 Grain-boundary diffusion can lead to rapid lengthening and thickening of grain boundary precipitates, especially by substitutional diffusion.

**The reason** for the transition from grain boundary allotriomorphs to Widmanstätten side-plates with increasing undercooling is not fully understood.

→ possible answer: **Relative Velocity of Incoherent & Semicoherent Interfaces vary with undercooling**

a) At small undercoolings, both semi-coherent and incoherent interfaces ~similar rates

b) At large undercoolings, only incoherent interfaces ~full use of increased driving force  
(Continuous growth)



\* **Intragranular ferrite in large-grained specimen**

: ferrite can also precipitate within the austenite grains (Fig. in page 17)  
suitable heterogeneous nucleation site ~ inclusions and dislocations  
generally **equiaxed** at low undercooling ↔ **more platelike** at higher undercoolings

# 5.6. The Precipitation of Ferrite from Austenite

Typical TTT curve for  $\gamma \rightarrow \alpha$  transformation  $\rightarrow f(t, T)$

J-M-A Eq.

$$f = 1 - \exp(-kt^n)$$

$k$ : sensitive with  $T$   $f(I, v) \sim \frac{\pi}{3} I v^3$   
 $n$ : 1 ~ 4 (depend on nucleation mechanism)

- a) Time for a given percentage transformation will decrease as the constant  $k$  increase
  - b)  $k$  increases with increases in  $\Delta T$  or total # of nucleation sites
- $\rightarrow$  Thus, decreasing the austenite grain size has the effect of shifting the C curve to shorter transformation times.

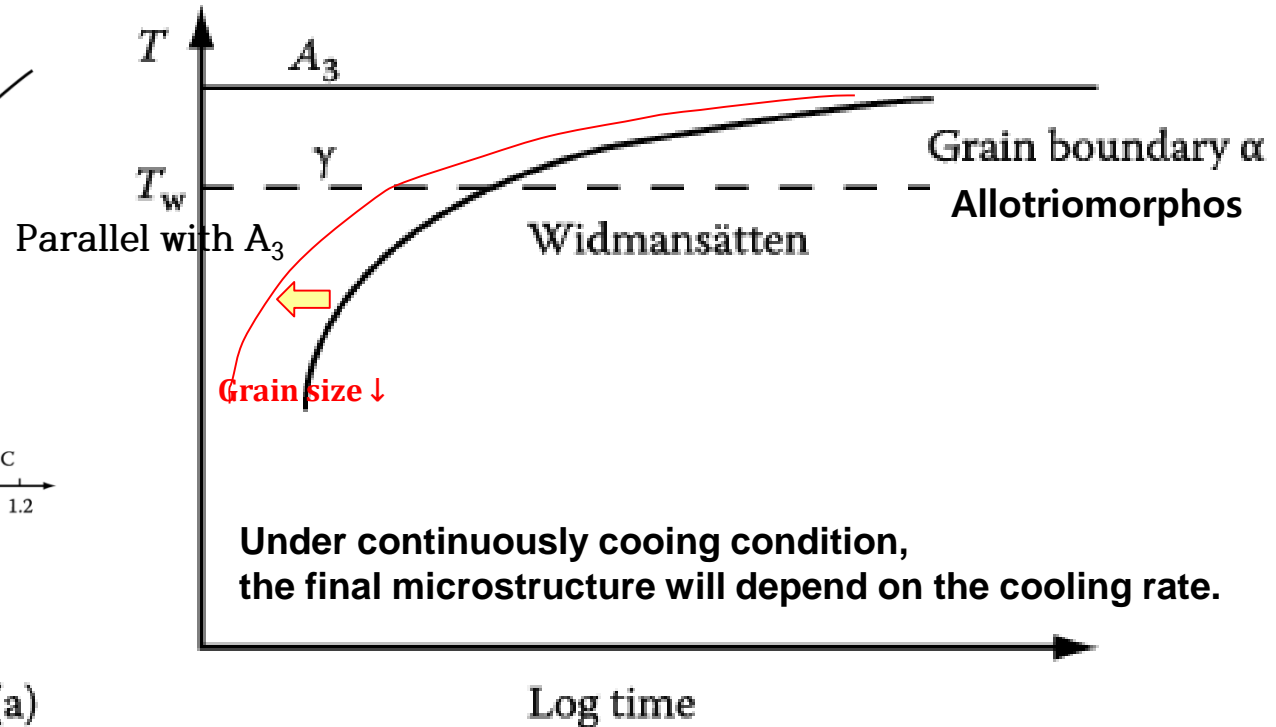
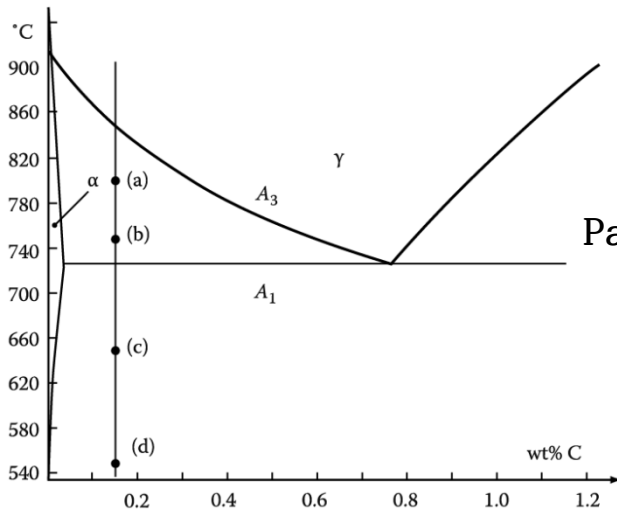
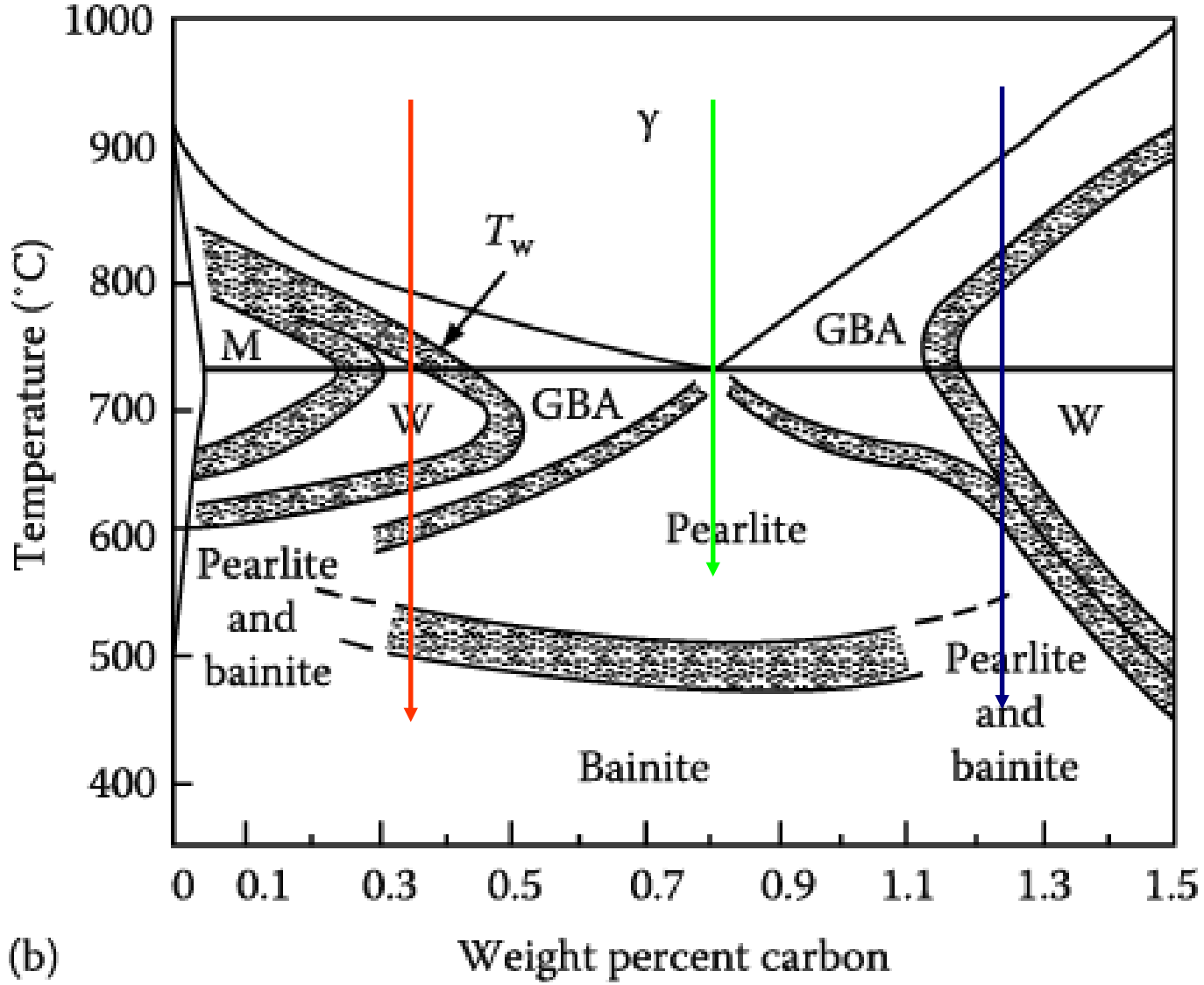


Figure 5.48 (a) typical TTT curve for  $\gamma \rightarrow \alpha$  transformation in a hypoeutectoid steel: a typical C shape.



For alloys of different carbon content,  $A_3$  and  $T_w$  vary and show parallel manner each other.



(GBA: GB allotriomorphs, W: Widmanstatten sideplates/intermolecular plates, M: Massive ferrite)

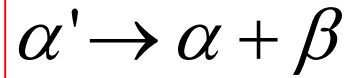
Figure 5.48 (b) Temperature-composition regions in which the various morphologies are dominant at late reaction times in specimens with ASTM grain size Nos. 0-1. 41

## **5.6.1 & 5.7 skip**

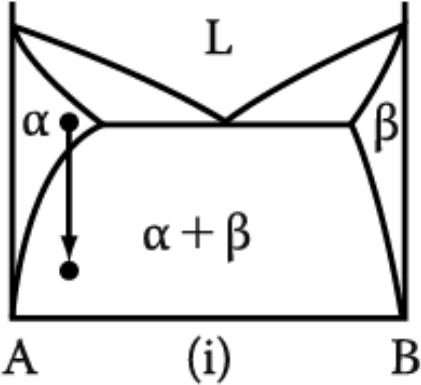
# 5. Diffusion Transformations in solid

: diffusional nucleation & growth

## (a) Precipitation



Metastable supersaturated  
Solid solution



### Homogeneous Nucleation

$$\Delta G = -V\Delta G_V + A\gamma + V\Delta G_S$$

### Heterogeneous Nucleation

$$\Delta G_{het} = -V(\Delta G_V - \Delta G_S) + A\gamma - \Delta G_d$$

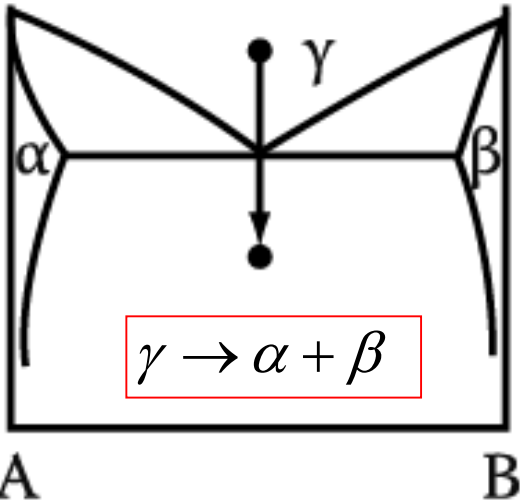
$$N_{hom} = \omega C_0 \exp\left(-\frac{\Delta G_m}{kT}\right) \exp\left(-\frac{\Delta G^*}{kT}\right)$$

→ suitable nucleation sites ~ nonequilibrium defects  
(creation of nucleus ~ destruction of a defect (-ΔG<sub>d</sub>))

## (b) Eutectoid Transformation

Composition of product phases  
differs from that of a parent phase.

→ long-range diffusion



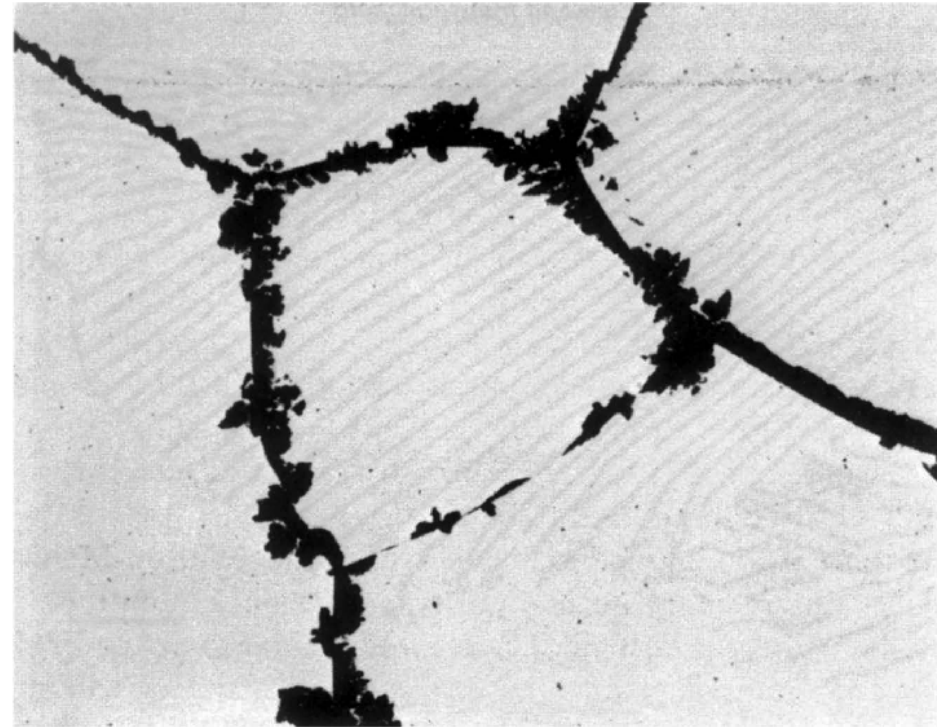
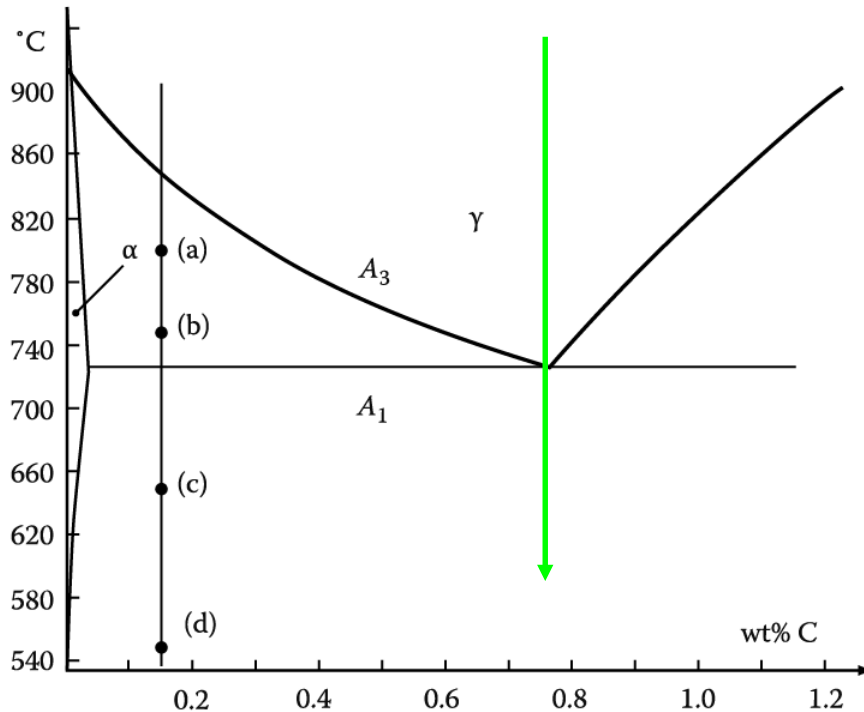
# 5.8. Eutectoid Transformation

## 5.8.1 Pearlite Reaction in Fe-C Alloys



Pearlite nodule nucleate on GBs and grow with a roughly constant radial velocity into the surrounding austenite grains.

Very similar to a eutectic transformation



\* **At large undercooling,**

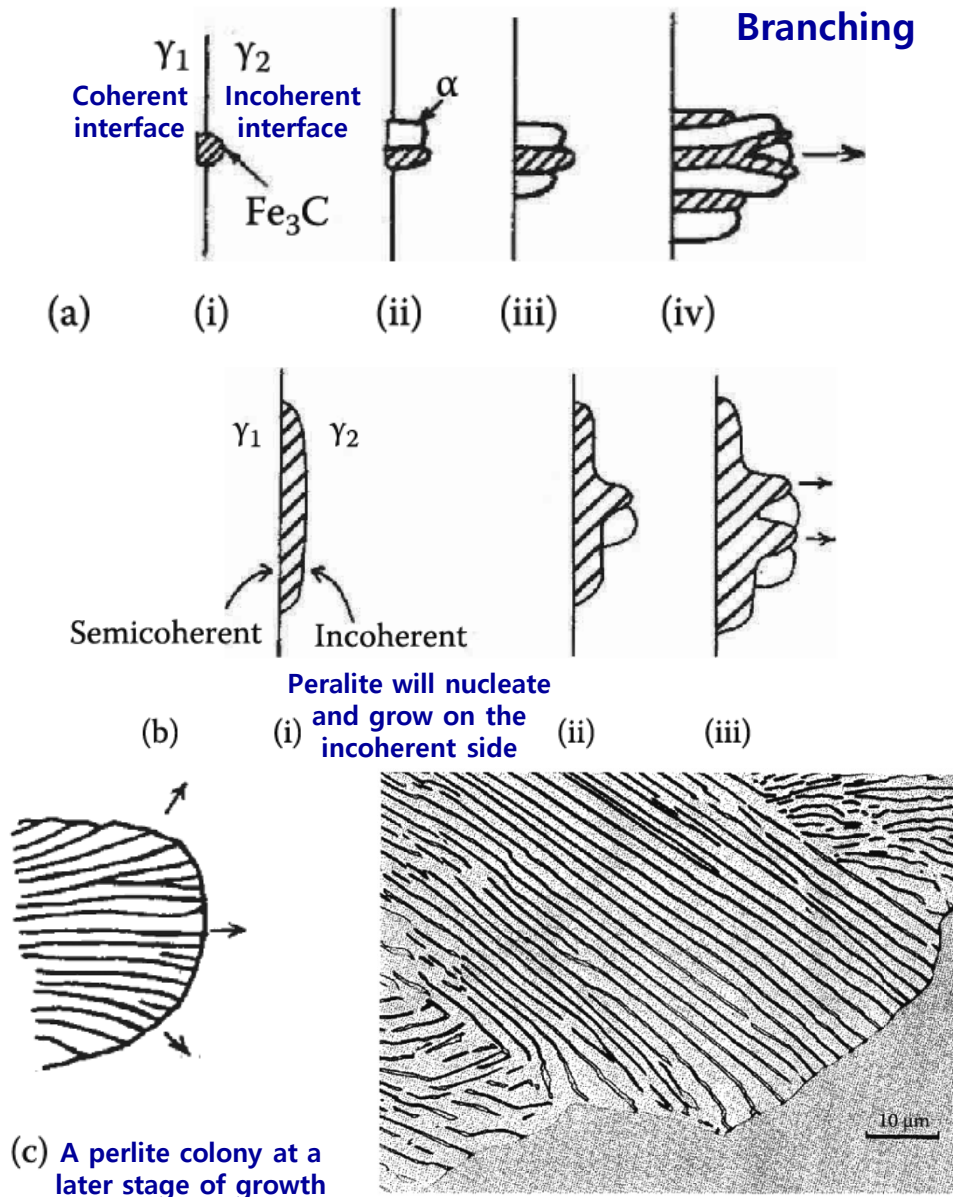
: the nucleation rate is much higher and site saturation occurs, that is all GBs become quickly covered with nodules which grow together forming layers of pearlite, Figure 5.61.

\* **At small undercooling below A<sub>1</sub>,**

: the number of pearlite nodules that nucleate is relatively small, and the nodules can grow as hemispheres or spheres without interfering with each other.

# Pearlite Reaction in Fe-C Alloys: nucleation and growth

**Nucleation:** depend on **GB structures and composition**



(a) On a “clean” GB.

- (i) **Cementite nucleates on GB** with coherent interface and orientation relationship with  $\gamma_1$  and incoherent interface with  $\gamma_2$ .
- (ii)  **$\alpha$  nucleates adjacent to cementite** also with a coherent interface and orientation relationship with  $\gamma_1$ . (This also produces an orientation relationship between the cementite and the ferrite).
- (iii) The **nucleation process repeats side ways**, while incoherent interfaces grow into  $\gamma_2$ .
- (iv) New plates can also form by a **branching** mechanism.

(b) When a proeutectoid phase (cementite or ferrite) already exists on that boundary, pearlite will **nucleate and grow on the incoherent side**. A different orientation relationship between the cementite and the ferrite results in this case.

(c) **Pearlite colony** at a latest stage of growth. Pearlite grows into the austenite grain with which it does not have an orientation relationship.

# Growth of Pearlite: analogous to the growth of a lamellar eutectic

Min. possible:  $(S^*) \propto 1/\Delta T$  / Growth rate : mainly lattice diffusion  $v = kD_c \gamma (\Delta T)^2$

Interlamellar spacing of pearlite colonies : mainly boundary diffusion  $v = kD_b (\Delta T)^3$

Relative Positions of the Transformation curves for Pearlite and Bainite in Plain Carbon Eutectoid Steels.

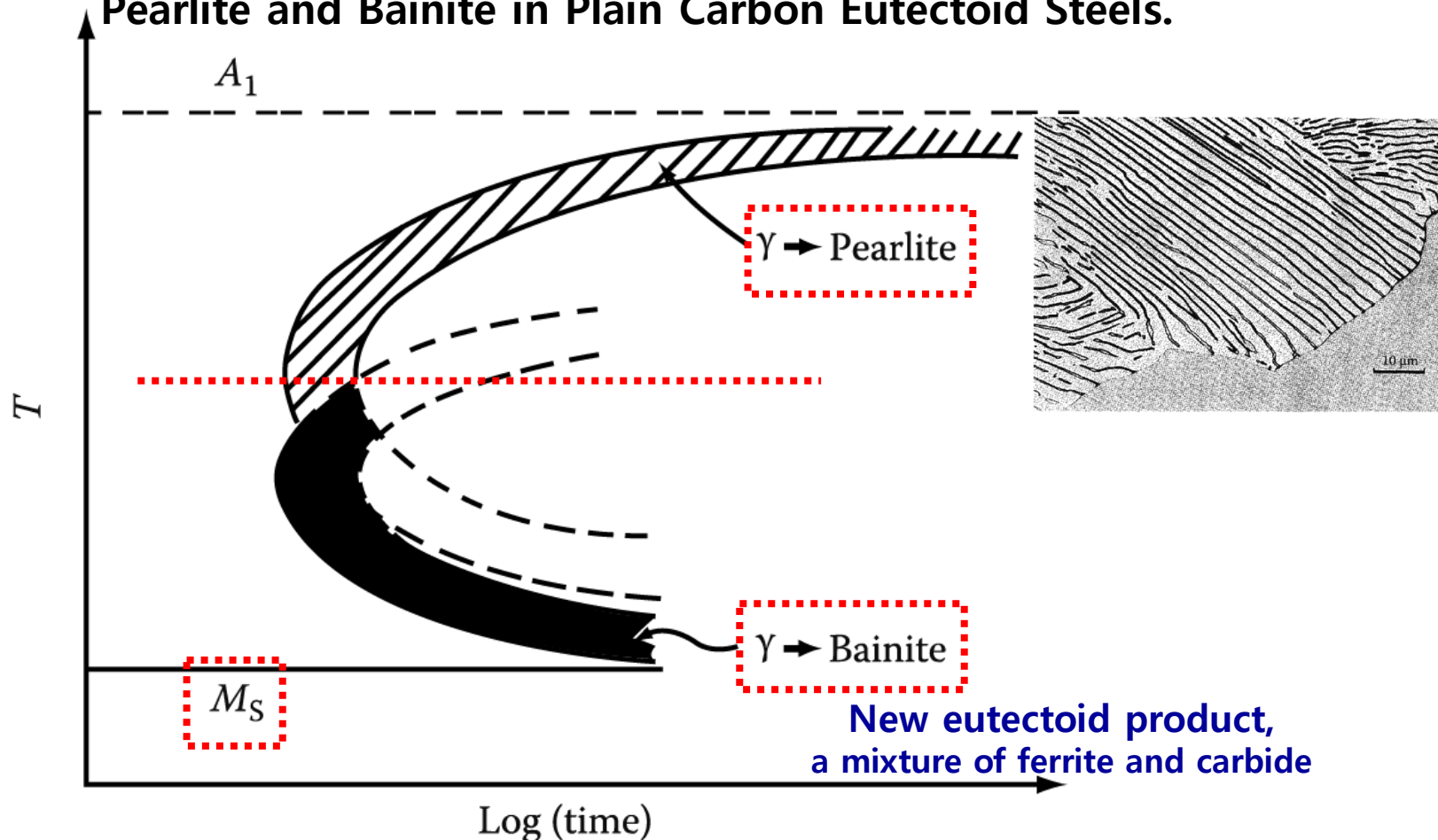


Figure 5.64 Schematic diagram showing relative positions of the transformation curves for pearlite and bainite in plain carbon eutectoid steel.



# 5.8.2 Bainite Transformation

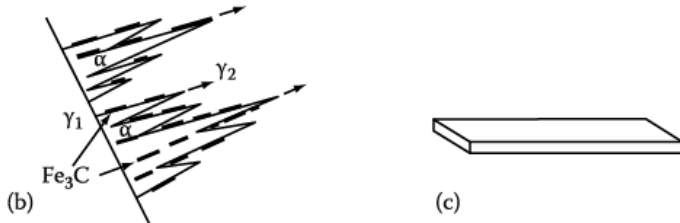
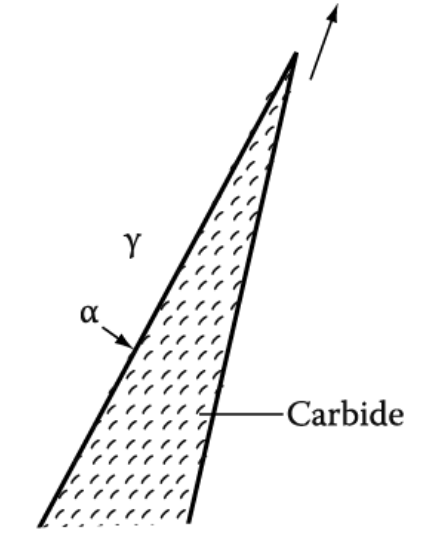
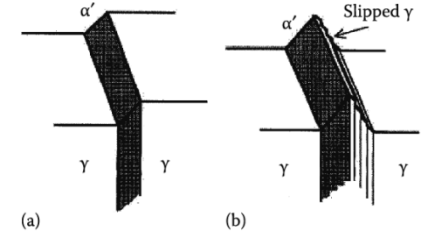
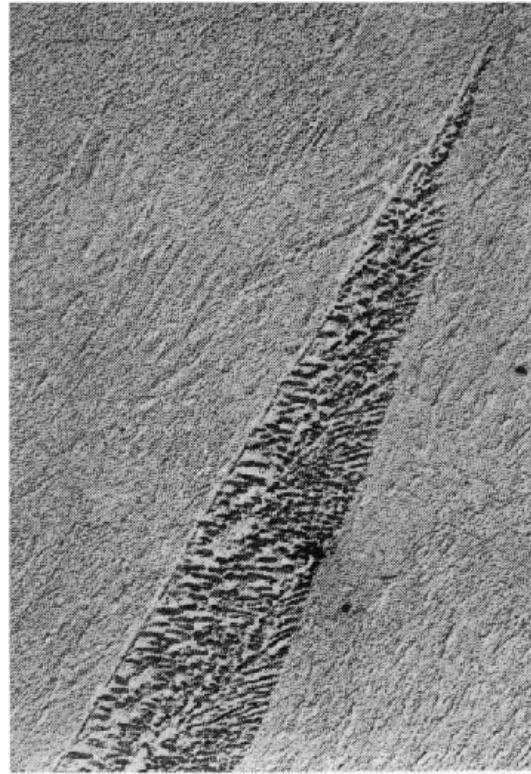
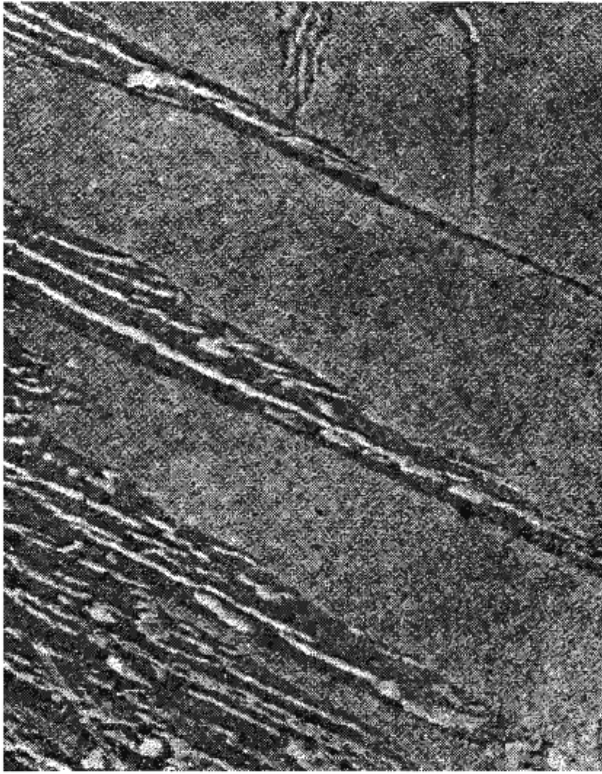
The microstructure of bainite depends mainly on the temperature at which it forms.

## Upper Bainite in medium-carbon steel

## Lower Bainite in 0.69wt% C low-alloy steel

At high temp. 350 ~ 550°C, ferrite laths, K-S relationship, similar to Widmanstätten plates

At sufficiently low temp. laths → plates  
Carbide dispersion becomes much finer, rather like in tempered M.



(a)

(b)

**Surface tilts by bainite trans. like M trans.  
Due to Shear mechanism/ordered military manner**

(b) Schematic of growth mechanism. Widmanstätten ferrite laths growth into  $\gamma_2$ . Cementite plates nucleate in carbon-enriched austenite.

(b) A possible growth mechanism.  $\alpha/\gamma$  interface advances as fast as carbides precipitate at interface thereby removing the excess carbon in front of the  $\alpha$ .

At the highest temp. where pearlite and bainite grow competitively.

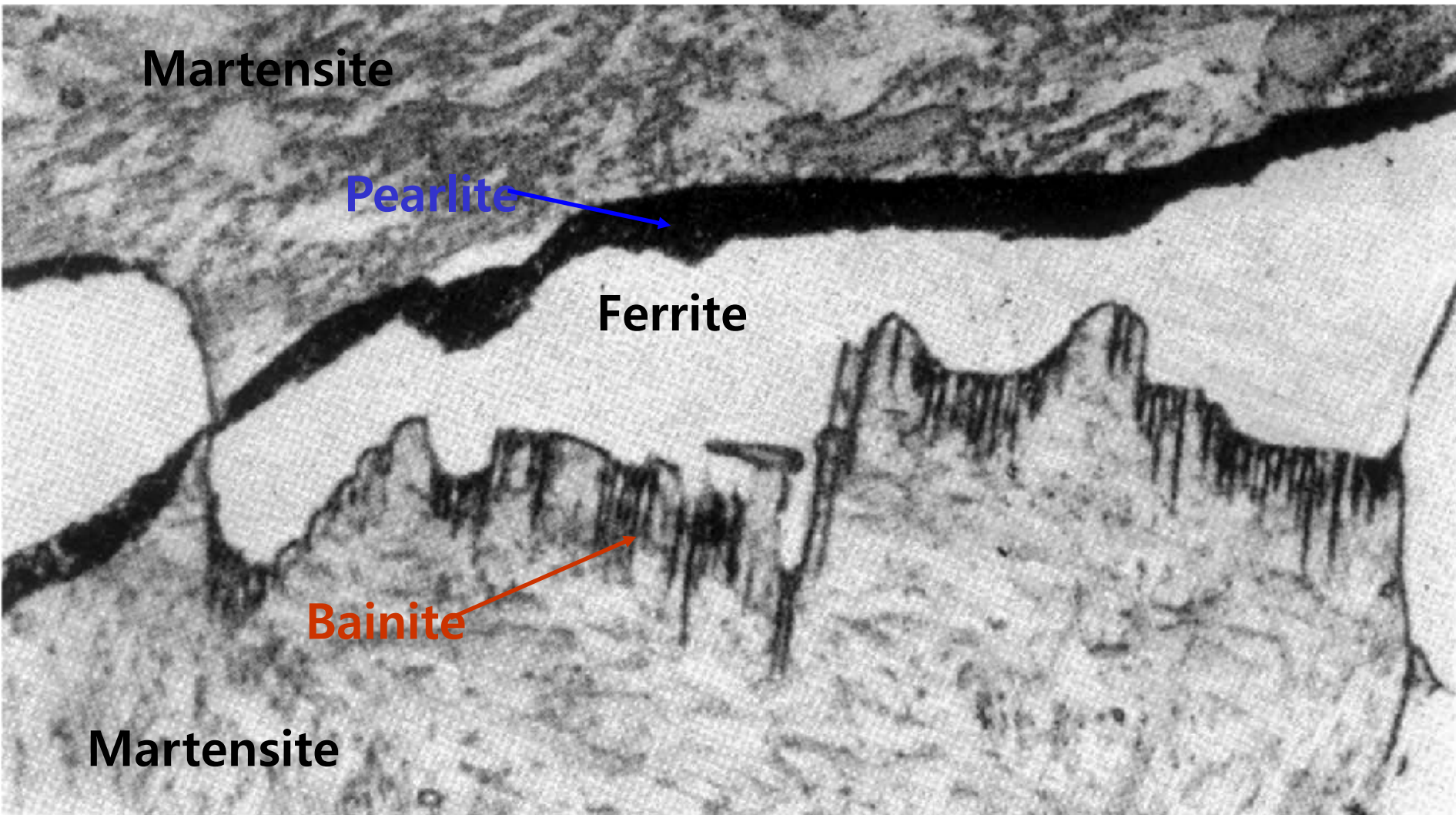


Fig. 5.67 Hypoeutectoid steel (0.6% C) partially transformed for 30 min at 710 °C. Inefficiently quenched. Bainitic growth into lower grain of austenite and pearlitic growth into upper grain during quench (x1800).

**Pearlite : no specific orientation relationship**

**Bainite : orientation relationship**



## 5.8.3 The effect of alloying elements on hardenability

: adding alloying elements to steels → delay to time required for the decomposition into ferrite and pearlite → M trans under slower cooling rate → increase hardenability

\* Main factor limiting hardenability is the rate of formation of pearlite at the nose of the C curve in the TTT diagram.

- Austenite stabilizer (Mn, Cu, Ni) – depress A3 temperature
- Ferrite stabilizer (Cr, Mo, Si) – increase A3 temperature

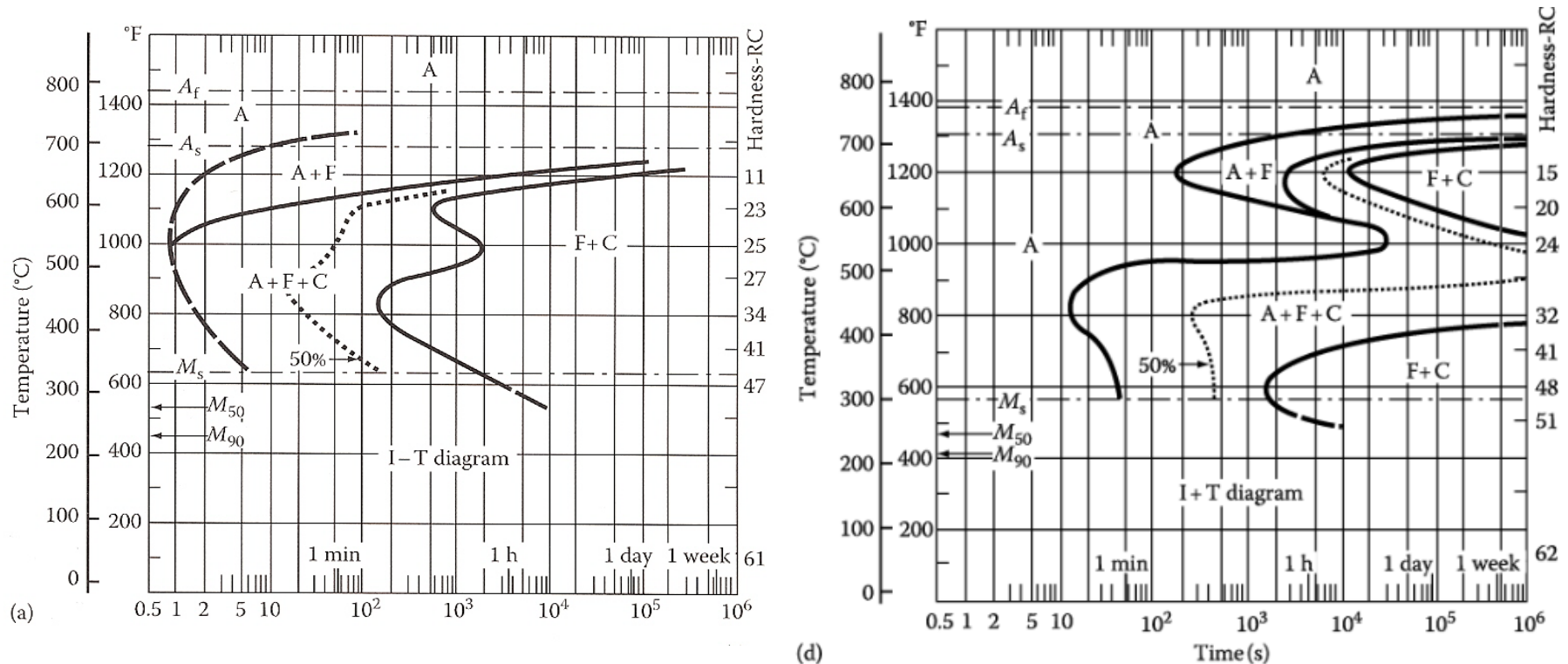
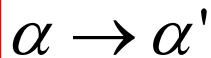


Figure 5.73 TTT diagrams for two commercial low-alloy steels all of which (a) contain roughly 0.4% C and 1% Mn and (b) contains 0.8% Cr, 0.3% Mo, and 1.8% Ni

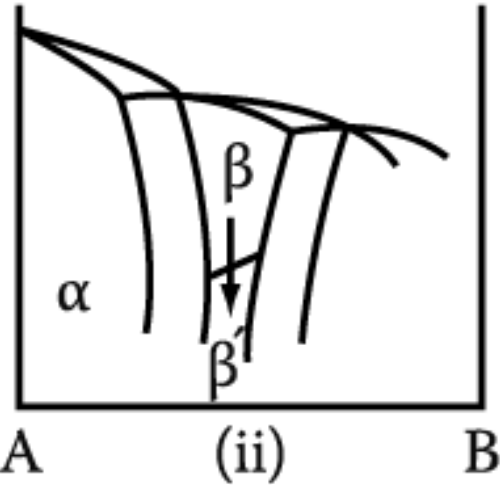
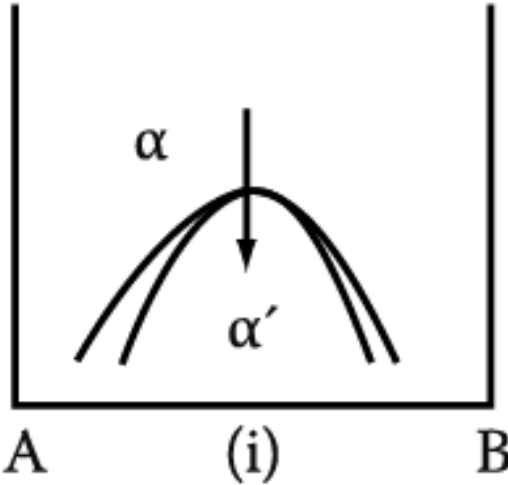
**5.8.4 - 5.8.6 skip**

# 5. Diffusion Transformations in solid

## (c) Order-Disorder Transformation

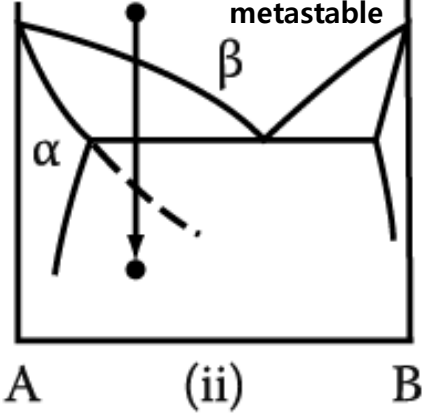
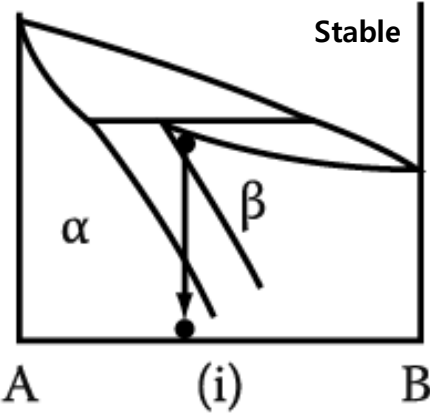


Disorder (high temp.)      Order (low temp.)



## (d) Massive Transformation

: The original phase decomposes into one or more new phases which have the same composition as the parent phase, but different crystal structures.

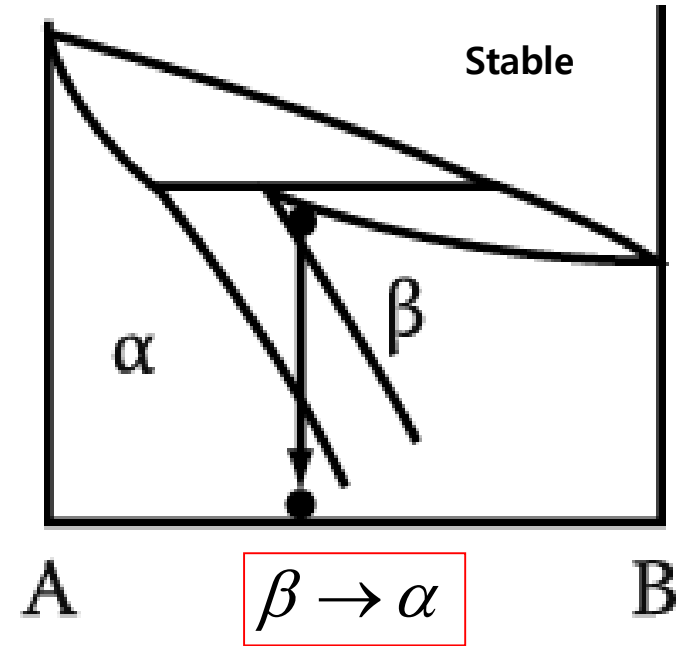
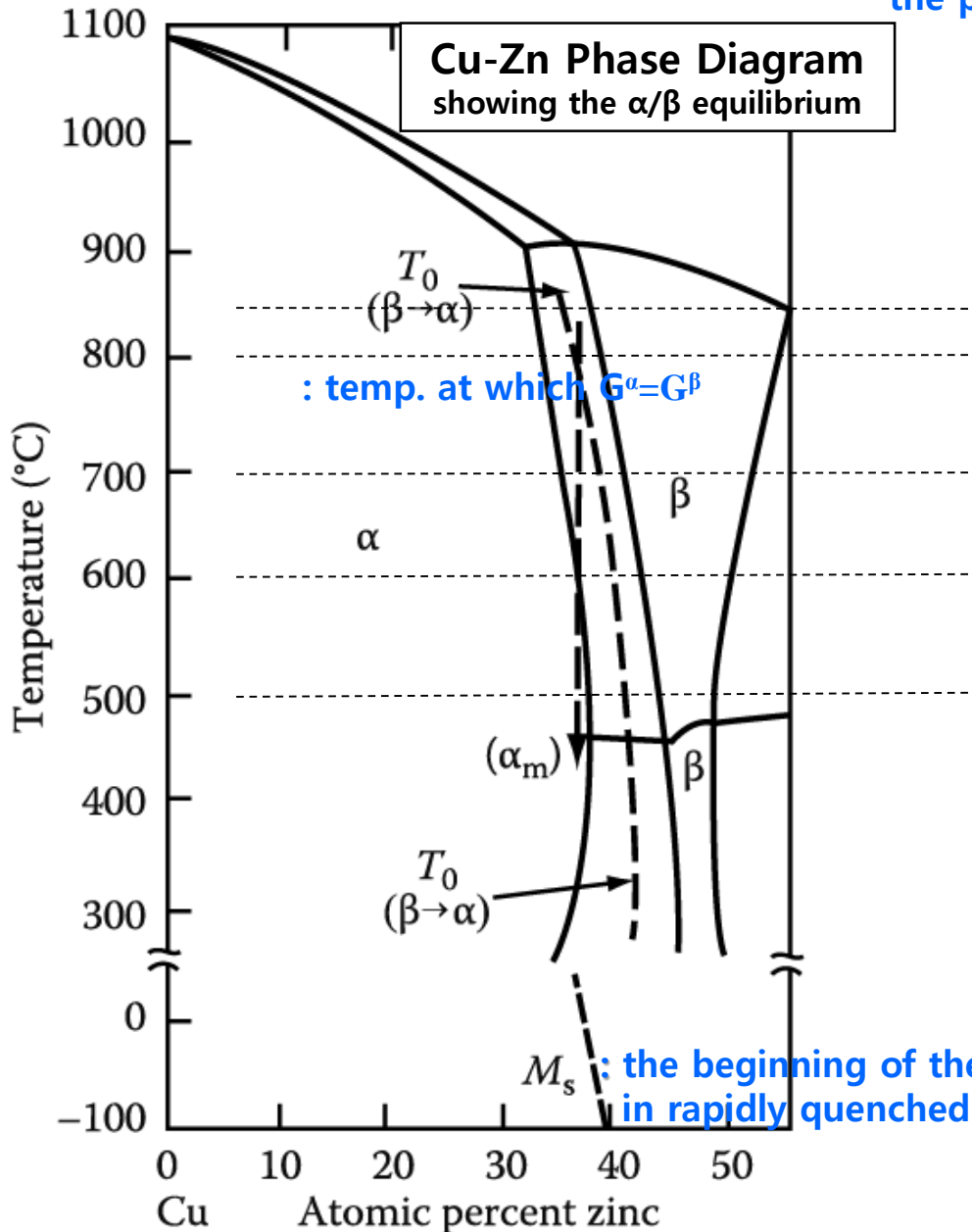


## (e) Polymorphic Transformation

In single component systems, different crystal structures are stable over different temperature ranges.



# 5.9 Massive Transformation: The original phase decomposes into one or more new phases which have the same composition as the parent phase, but different crystal structures.



**Free energy-composition curves for  $\alpha$  and  $\beta$  at 850 $^{\circ}\text{C}$ , 800 $^{\circ}\text{C}$ , 700 $^{\circ}\text{C}$  and 600 $^{\circ}\text{C}$ ?**

# 5.9 Massive Transformation

## Free energy-composition curves for $\alpha$ and $\beta$

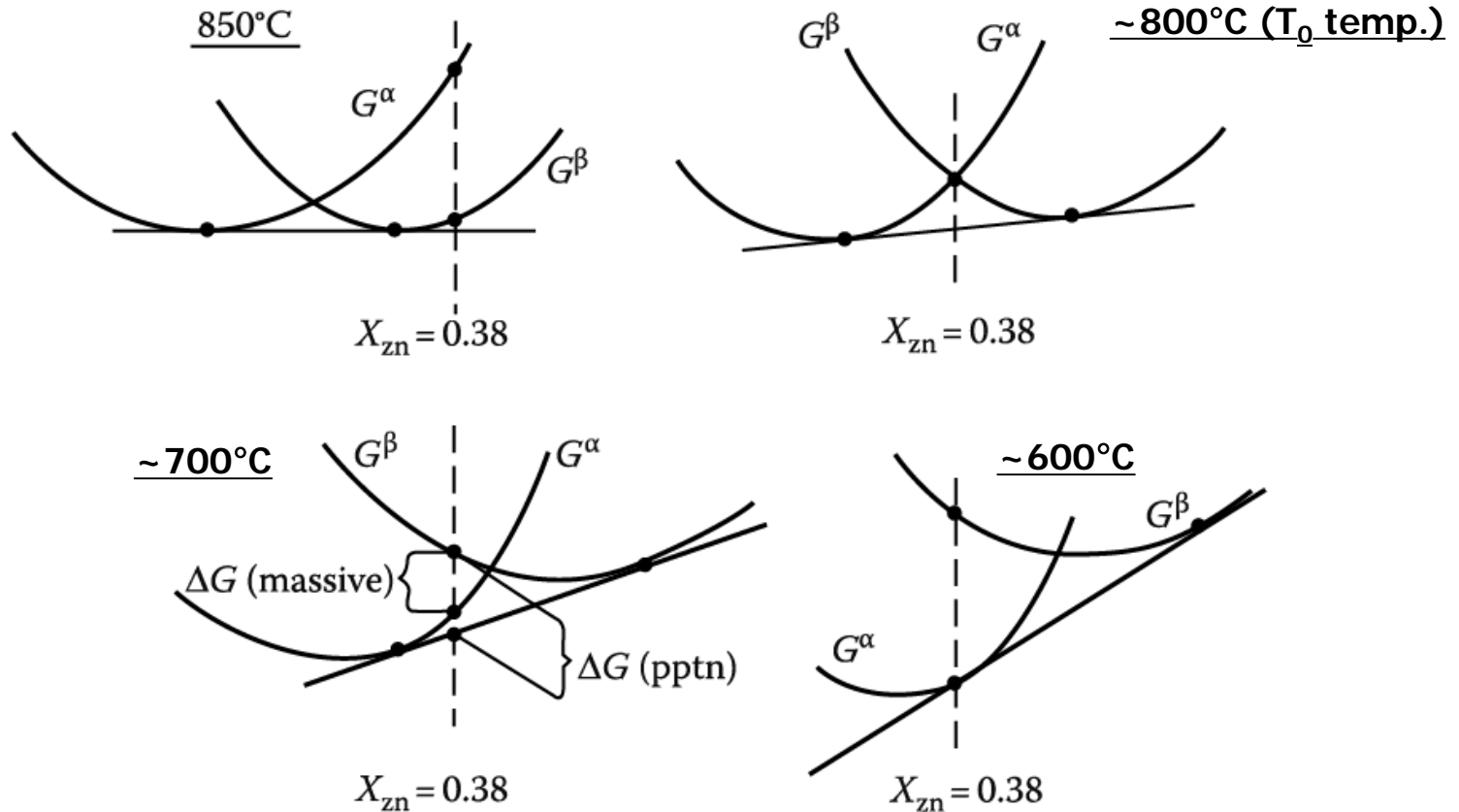


Fig. 5.86 A schematic representation of the free energy-composition curves for  $\alpha$  and  $\beta$  in the Cu-Zn system at various temperatures.

At the thermodynamic point of view, it may possible for a massive trans. to occur within the two-phase region of the phase dia. anywhere below the  $T_0$  temp.. But, in practice, there is evidence that massive trans. usually occur only within the "single-phase region" of the phase diagram

## 5.9 Massive Transformation

Massive  $\alpha$  formed at the GBs of  $\beta$  and grow rapidly into the surrounding  $\beta$

: a diffusionless civilian transformation (change of crystal structure without a change of composition)

Migration of the  $\alpha/\beta$  interfaces~ very similar to the migration of GBs during recrystallization of single-phase material but, driving force ~ orders of magnitude greater than for recrystallization→ rapid growth: a characteristic irregular appearance.

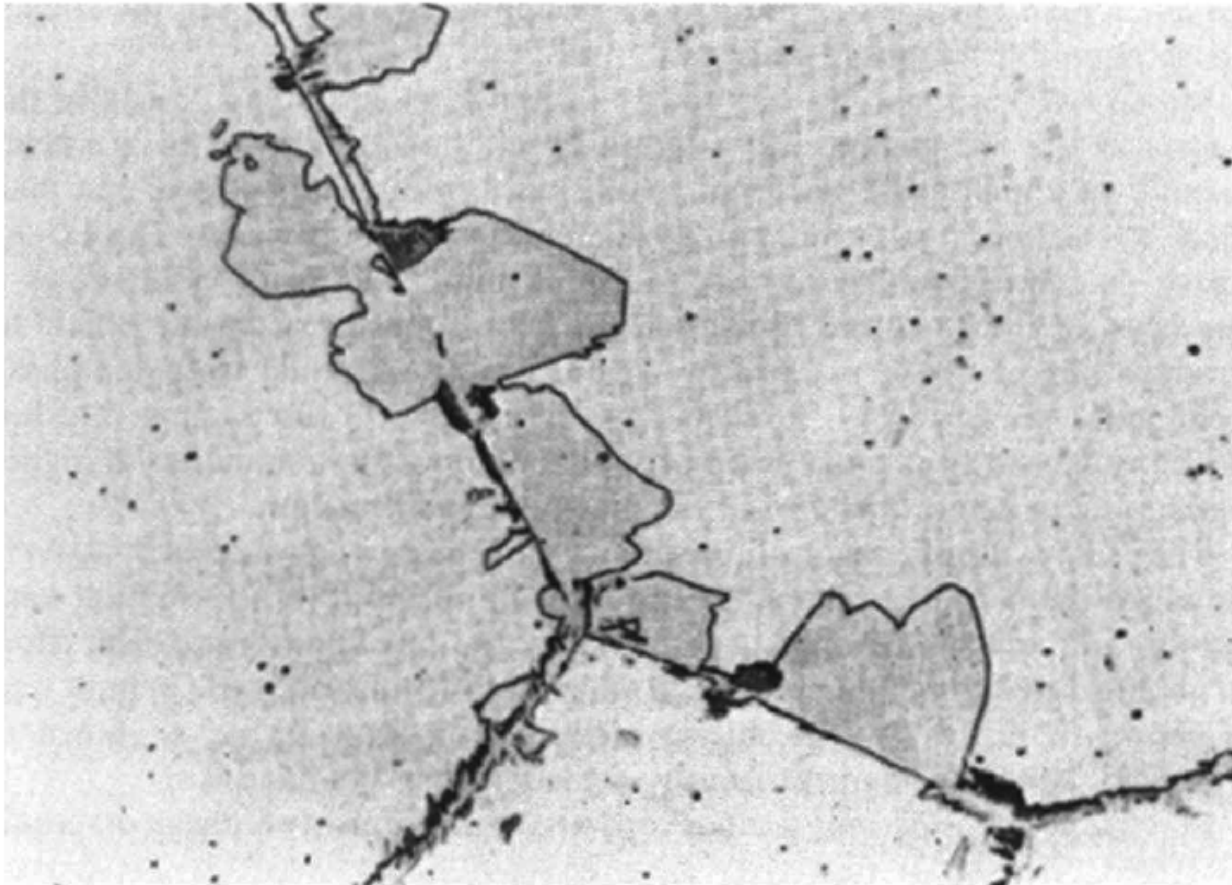
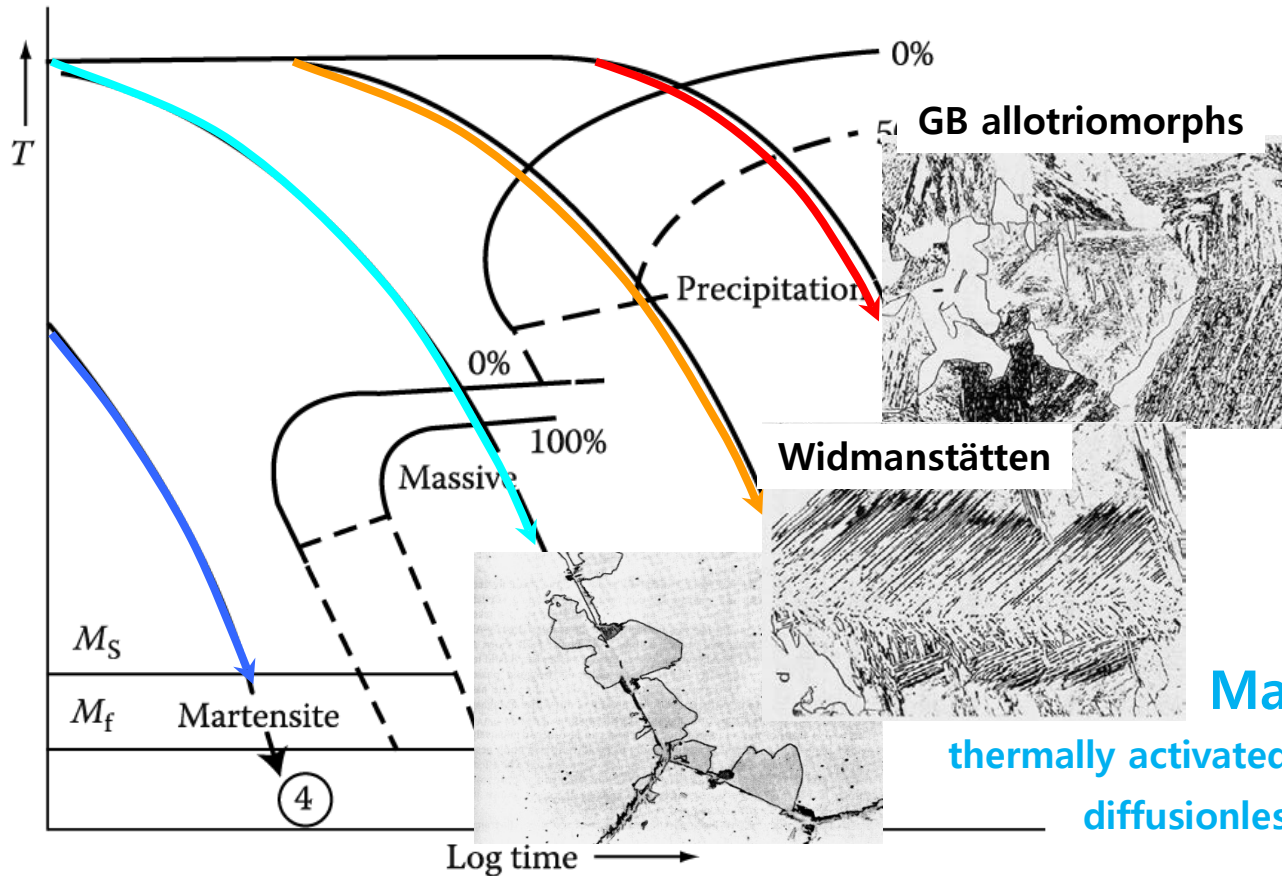


Figure 5.85 Massive  $\alpha$  formed at the GBs of  $\beta$  in Cu-38.7wt% Zn quenched from 850°C in brine at 0°C. Some high temperature precipitation has also occurred on the boundaries.



# \* Massive, Martensite Transformation



## Massive Transformation

thermally activated jumping across the  $\alpha/\beta$  interface

diffusionless civilian transformation



$\beta$  is sheared into  $\alpha$  by the cooperative movement of atoms across a glissile interface

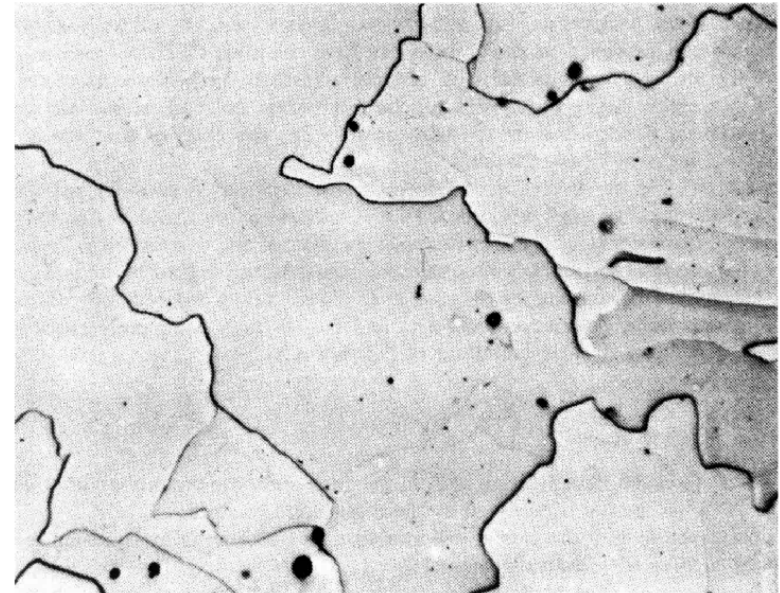
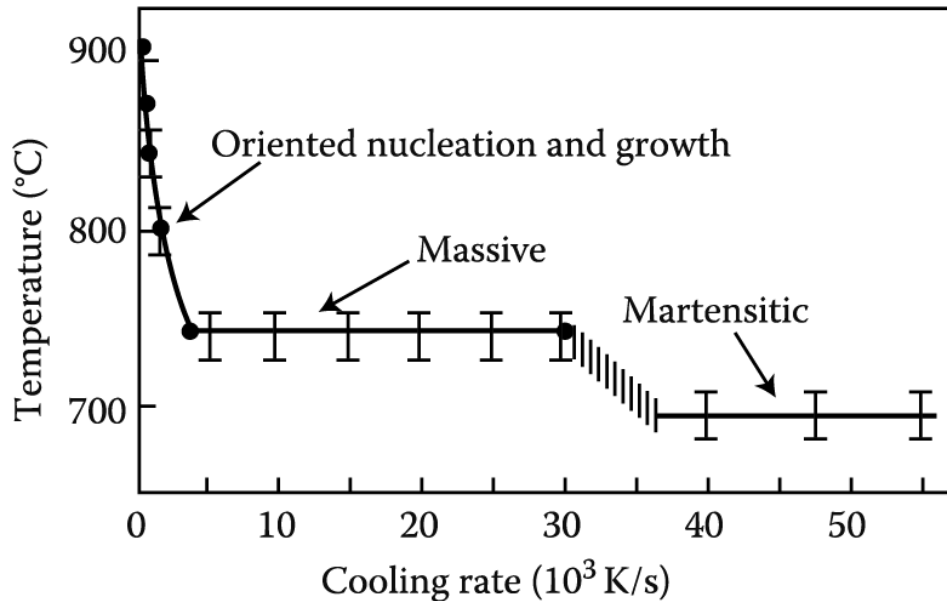
diffusionless military transformation

## Martensite Transformation

Fig. 5.75 A possible CCT diagram for systems showing a massive transformation. Slow cooling (1) produces equiaxed  $\alpha$ . Widmanstätten morphologies result from faster cooling (2). Moderately rapid quenching (3) produces the massive transformation, while the highest quench rate (4) leads to a martensitic transformation.

# 5.9 Massive Transformation: $\gamma \rightarrow \alpha$ transformation in iron and its alloy

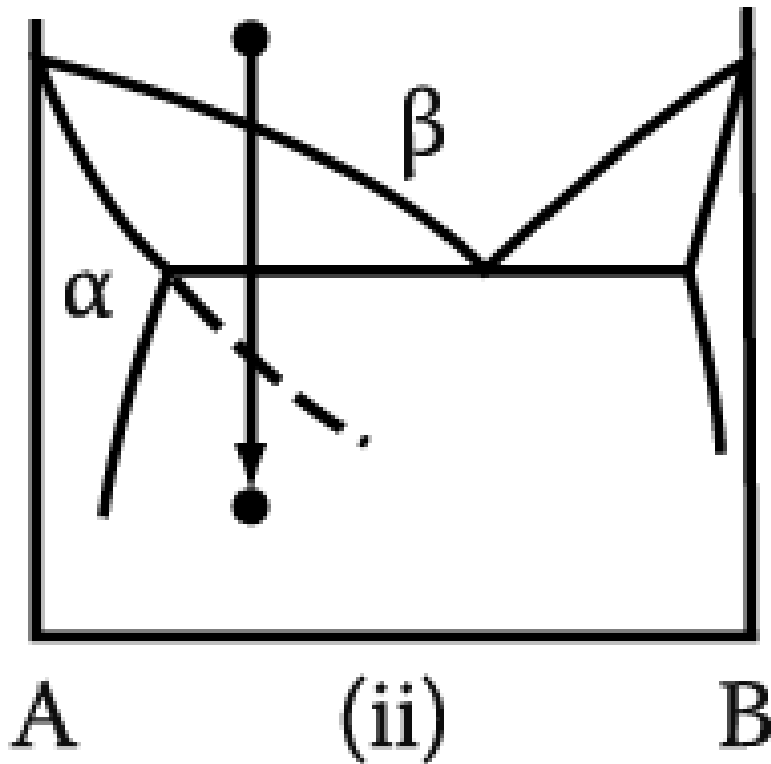
## Effect of Cooling Rate on the Transformation Temperature at which transformation starts in pure iron



**Massive  $\alpha$  in an Fe-0.002wt%C**  
Quenched into iced brine from 1000 °C  
: characteristically irregular  $\alpha/\alpha$  GBs.



## 5.9 Massive Transformation



**Metastable phases can also form massively.**

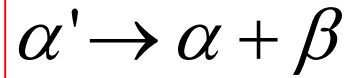
It is not even necessary for the transformation product to be a single phase: **two phases, at least one of which must be metastable**, can form simultaneously provided they have the same composition as the parent phase.

## **5.10 & 5.11 skip**

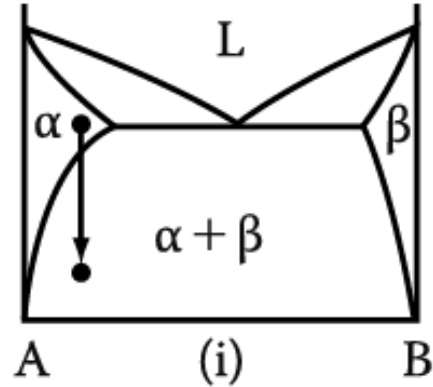
# 5. Diffusion Transformations in solid

: diffusional nucleation & growth

## (a) Precipitation



Metastable supersaturated  
Solid solution



### Homogeneous Nucleation

$$\Delta G = -V\Delta G_V + A\gamma + V\Delta G_S$$

### Heterogeneous Nucleation

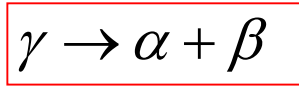
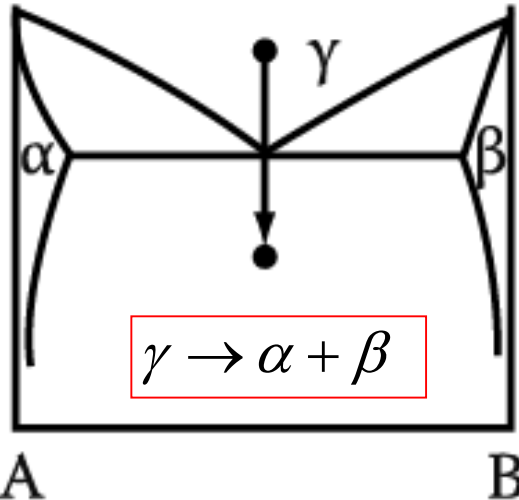
$$\Delta G_{het} = -V(\Delta G_V - \Delta G_S) + A\gamma - \Delta G_d$$

$$N_{hom} = \omega C_0 \exp\left(-\frac{\Delta G_m}{kT}\right) \exp\left(-\frac{\Delta G^*}{kT}\right)$$

→ suitable nucleation sites ~ nonequilibrium defects  
(creation of nucleus ~ destruction of a defect (-ΔG<sub>d</sub>))

## (b) Eutectoid Transformation

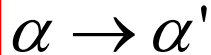
Composition of product phases  
differs from that of a parent phase.  
→ long-range diffusion



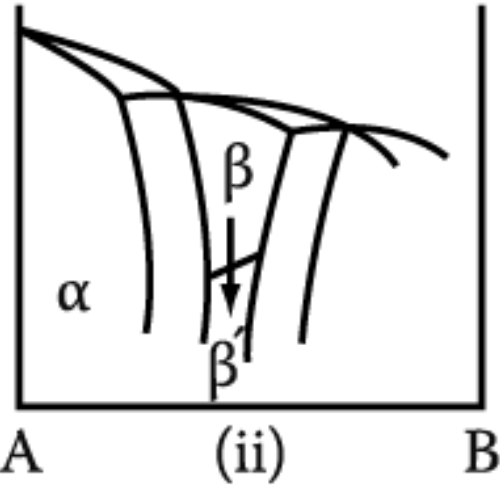
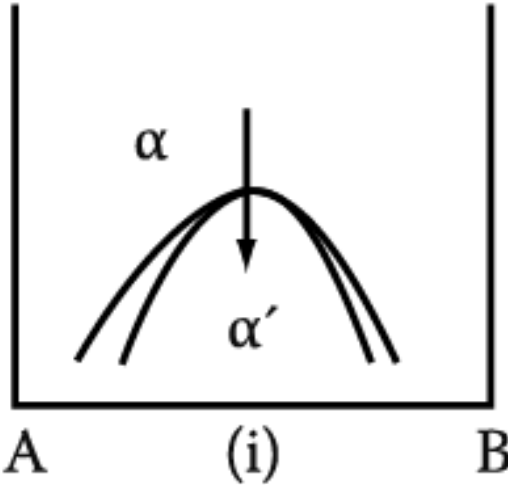
Which transformation proceeds  
by short-range diffusion?

# 5. Diffusion Transformations in solid

## (c) Order-Disorder Transformation

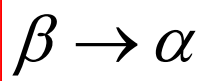
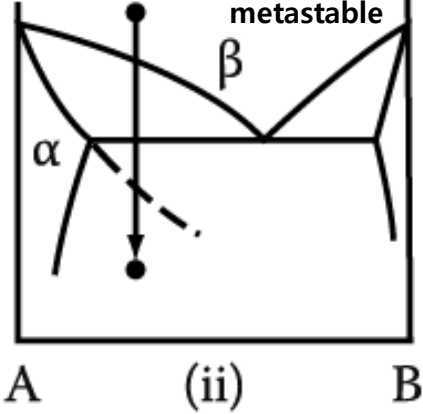
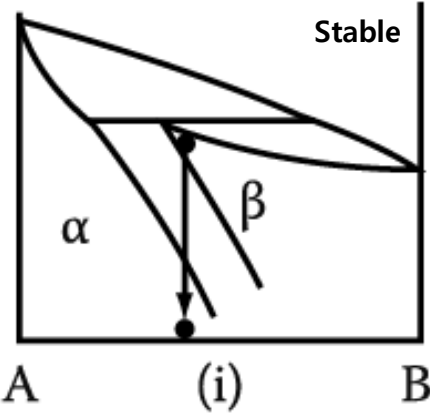


Disorder (high temp.)      Order (low temp.)



## (d) Massive Transformation

: The original phase decomposes into one or more new phases which have the same composition as the parent phase, but different crystal structures.



## (e) Polymorphic Transformation

In single component systems, different crystal structures are stable over different temperature ranges.



**\* Homework 5 : Exercises 5 (pages 379-381)**

**until 10th December**

**Good Luck!!**